APPLIED ENERGY

5th Generation District Heating: A novel design approach based on mathematical optimization

Marco Wirtz, Lukas Kivilip, Peter Remmen, Dirk Müller

***RWTH Aachen University**, E.ON Energy Research Center, Institute for Energy Efficient Buildings and Indoor Climate, Mathieustr. 10, Aachen, Germany*

Full journal article: https://www.sciencedirect.com/science/article/pii/S0306261919318458

DOI: 10.1016/j.apenergy.2019.114158

Accepted manuscript

5th Generation District Heating: A novel design approach based on mathematical optimization

Marco Wirtz[a,*], Lukas Kivilip[a], Peter Remmen[a], Dirk Müller[a]

[a] *RWTH Aachen University, E.ON Energy Research Center, Institute for Energy Efficient Buildings and Indoor Climate, Mathieustr. 10, Aachen, Germany*

Abstract

This paper presents a novel design methodology based on Linear Programming for designing and evaluating distributed energy systems with bidirectional low temperature networks (BLTNs). The mathematical model determines the optimal selection and sizing of all energy conversion units in buildings and energy hubs connected to the BLTN while minimizing total annualized costs. The optimization superstructure of building energy systems comprises heat pumps, compression chillers, heat exchangers for direct cooling, cooling towers and thermal energy storages. The design approach is applied to a real-world use case in Germany and the BLTN performance is compared to a reference case with individual HVAC systems. The BLTN concept shows a cost reduction of 42 % and causes 56 % less CO_2 emissions compared to individual HVAC systems.

Keywords:

Bidirectional low temperature network, District heating, District cooling, Waste heat, Prosumer, Linear Programming

*Corresponding author

Email address: marco.wirtz@eonerc.rwth-aachen.de (Marco Wirtz)

1. Introduction

With 50 % of final energy consumption, heating and cooling is the largest energy sector in Europe [1]. While the heating demand is expected to decrease, the cooling demand in buildings will increase substantially in the upcoming decades [2]. The task of an emission-free supply of heating and cooling energy is challenging, especially in urban areas: Space is a very limited resource and noise emissions should be kept to a minimum. An energy supply by individual supply units in buildings is therefore not satisfying. Instead, district heating and cooling (DHC) gains more importance. DHC networks enable an efficient energy supply while reducing primary energy demands as well as local emissions [3]. In order to increase the efficiency of thermal networks, a tendency towards lower operating temperatures is observed [4]. Lower network temperatures reduce thermal losses and enable the integration of low-grade waste heat and renewable heat sources ([5], [6]).

The latest innovation in district heating are 5th Generation District Heating and Cooling networks. In the following, a brief literature review on this technology is provided and relevant gaps for this work are identified.

1.1. 5th Generation District Heating and Cooling

The latest stage in the development of DHC systems are *5th Generation District Heating and Cooling* (5GDHC) networks ([7], [8]). In literature, these networks are also referred to as *Bidirectional Low Temperature Networks* ([9], [10], [11], [12]), *Cold District Heating Networks* (in German *Kalte Nahwärme*) ([13], [14]) or *Anergy Networks* ([15], [16], [17]) (in Ger-

man *Anergienetze*). In this study, they are referred to as *Bidirectional Low Temperature Networks* (BLTN). The general concept of BLTNs is depicted in Fig. 1. Heating and cooling consumers are connected to a thermal network which consists of a warm and a cold pipe. The temperature of the fluid in the warm pipe is around 5 – 10 K higher than the temperature in the cold pipe. The temperatures in both pipes are close to the surrounding (5 °C – 30 °C), which keeps heat losses to a minimum. In order to raise the temperature level for space heating or domestic hot water, buildings are equipped with heat pumps. Heat pumps use water from the warm pipe as heat source. Cooled water from the evaporator is then discharged into the cold pipe. Likewise, chillers use the network as heat sink. They take water from the cold pipe and discharge the heated fluid into the warm pipe. Thus, the flow direction of the water in the network can change over time in each segment of the network and only depends on the operation of the decentralized pumps in the buildings. One key advantage is that low-grade waste heat (e.g. from space cooling) can be directly fed into the warm pipe without raising its temperature with additional equipment. This enables the efficient recovery of local low-grade waste heat ([18], [19]). In districts where heating and cooling demands are about the same magnitude, a substantial proportion of thermal demands can be balanced out by the BLTN. The unbalanced, remaining thermal demands have to be covered by additional supply units, like energy hubs or conventional DHC infrastructure. The extensive use of heat pumps and chillers in buildings supports balancing fluctuations in the power grid, which result from increasing penetration of renewable energy generation [20]. A comprehensive review on BLTNs is presented by Buffa et al. [7] and Boesten

et al. [21]. The potential of BLTNs for economic and ecological savings has been demonstrated in recent studies ([9], [22], [23], [24], [25], [26], [27]).

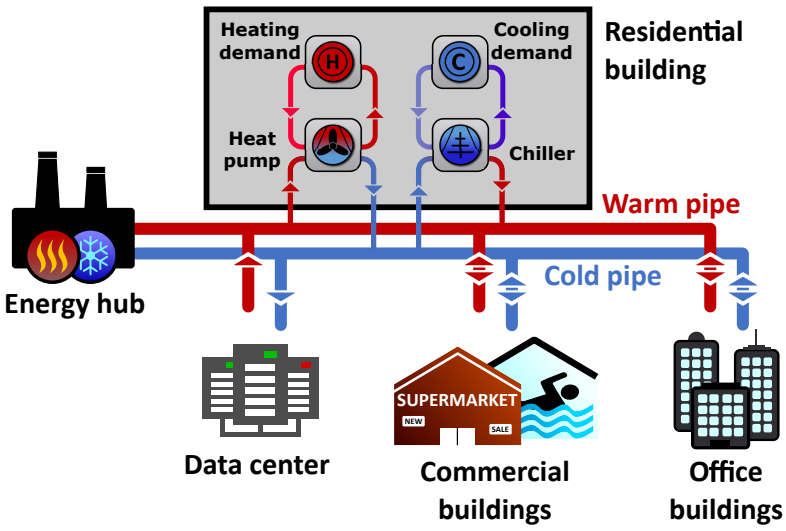

Figure 1: Overview of different heating and cooling prosumers connected to a bidirectional low temperature network. Heat pumps in buildings use the network as heat source. For chillers the network serves as heat sink.

Ruesch et al. [28] emphasize the need for optimization approaches due to a lack of established design guidelines: On building level, the building energy system needs to be designed and sized. On network level, determining an optimal topology and pipe sizing is another major optimization task.

In literature, designing distributed energy systems with thermal networks has already been extensively investigated. In the following section, an overview of the current state of research is provided and existing gaps relevant in the context of BLTNs are highlighted.

1.2. Optimization of distributed energy systems

Due to the mutual heat exchange and interaction between buildings in districts with BLTNs, it is not sufficient to design building energy systems individually. Instead, the design problem (technology selection and sizing of all components) has to be addressed holistically for all buildings in a district. However, designing multiple thermally coupled building energy systems is a challenging task and calls for optimization methods. Holistic design approaches for districts with district heating infrastructure have been widely investigated in scientific literature. In this field, besides genetic algorithms, mathematical optimization (most commonly mixed-integer linear programs (MILP)) is considered the most promising approach.

Mehleri et al. [29] present a MILP formulation for the optimal design of distributed energy systems for small neighborhoods. From a superstructure containing different technologies, like micro CHPs, boilers or thermal storages, the optimal set is selected for each building. In contrast to the BLTN concept, heat from the network can directly cover the buildings' heat demand and no heat pumps for waste heat recovery are considered.

Harb et al. [30] formulate a similar MILP adding further technologies to the superstructure, such as photovoltaics (PV) and air source heat pumps (ASHP). They consider conventional district heating networks. Similar formulations are presented by Wouters et al. [31], Wu et al. [32] and Omu et al. [33]. All aforementioned studies do not consider district cooling networks or waste heat recovery.

In numerous studies, cooling networks have been considered in addition to district heating: Yang et al. [34] present a MILP formulation that includes

conventional district heating and cooling networks with two separate circuits. The optimal equipment of the building energy systems is selected and sized. However, no heat pumps in the buildings are considered.

Wouters et al. [35] propose an enhanced superstructure that includes a trigeneration system on building level by considering micro CHPs, absorption chillers and thermal storages. Again, conventional DHC networks with two separated circuits are considered.

Mashayekh et al. [36] present another MILP formulation for optimizing multi-energy microgrids with a multi-node modeling approach. Within the optimization different nodes are connected by conventional DHC networks.

A comprehensive review of optimization approaches for distict heating systems is provided by Sameti et al. [37]. However, in none of the aforementioned studies, BLTNs or waste heat recovery with heat pumps have been addressed.

However, in different application contexts, mathematical optimization models have been presented which include these aspects: Bohlayer et al. [38] propose a MILP formulation for the economic optimization of an energy supply system that includes waste heat recovery and heat pumps. However, the model was formulated for the energy system of a manufacturing company in which waste heat from hot process streams and refrigeration cycles are utilized. No urban energy system with BLTN is considered.

All in all, it appears that there has been no optimization model presented for designing distributed energy systems with BLTNs. This paper aims at closing this gap. In the following section, the contributions of this paper are presented in detail.

1.3. Contributions

In this paper, a superstructure-based deterministic LP model for designing distributed energy systems with BLTNs is presented. The design approach is applied to a real-world use case. The BLTN solution is compared to an alternative supply concept with stand-alone HVAC systems. Both concepts are evaluated with thermodynamic, economic and environmental performance indicators.

The major contributions of this paper are:

- A novel mathematical optimization formulation for designing district energy systems with BLTNs in the early planning phase is presented.
- A novel optimization superstructure for building energy systems connected to a BLTN is investigated: For covering heating demands, heat pumps, electric boilers and heat storages are available. For cooling supply, compression chillers, cooling towers and heat exchangers for direct cooling with the cold pipe of the BLTN are considered.
- Evaluation of a BLTN and comparison with an alternative supply concept with individual HVAC systems with respect to total annualized costs, environmental impact and exergy efficiency.

1.4. Paper organization

This paper is structured as follows: In Section 2, the formulation of the Linear Program is presented (Section 2.1), the main assumptions and limitations are highlighted (Section 2.2) and the thermodynamic, economic and environmental indicators for evaluating the system performance are introduced (Section 2.3). In Section 3, a real-world use case with 17 buildings is

presented. The results of the case study are elaborated in Section 4. Finally, conclusions and outlooks are provided in Section 5.

2. Methodology

2.1. LP formulation

In this section, the Linear Program (LP) is presented in full detail. The LP formulation seeks to determine the optimal energy supply system to cover time-varying heating and cooling demands of buildings in a district with a BLTN. The optimization method selects and sizes energy conversion and storage units in all buildings and determines their optimal operation. The operation assumes perfect foresight of future demands and weather conditions and no operation strategy is prescribed. The main constraint of the system is to cover the heating and cooling demands of all buildings at every time step. In this study, the duration of all time steps is $\Delta t = 1$ hour, since this interval lengths provides a good trade-off regarding accuracy and computing times [39]. Power demands of appliances in buildings not related to the thermal energy system, such as lighting, are not considered since the investigations focus on the optimal heating and cooling supply.

The optimization model is based on time series for one year. In a preprocessing step, the annual time series are clustered into design days. For the clustering process, the k-medoids algorithm is used as presented by Domínguez et al. [40] and implemented by Schütz et al. [39].

In the model, two superstructures are considered: one for the energy hub (EH) and one for the building energy systems (BESs). All decision variables of the model are constrained to have non-negative values unless

otherwise stated. The model description is subdivided as follows: First, the objective function and related cost shares are presented. Subsequently, all model constraints of the BESs, the thermal network and the EH are described.

2.1.1. Objective function

The presented LP aims at determining the optimal energy system for all buildings connected to the BLTN as well as the energy hub while minimizing the total annualized costs (TAC). The definition of the TAC is based on the German guideline VDI 2067 [41] and includes annualized costs for the equipment of the energy hub (C_{EH}), the building energy systems (C_{BES}) and the network infrastructure (C_{netw}) as well as gas and electricity costs (C_{gas}, C_{el}) and revenues from electricity feed-in ($R_{\mathrm{feed-in}}$):

$$TAC = C_{\mathrm{EH}} + C_{\mathrm{BES}} + C_{\mathrm{gas}} + C_{\mathrm{el}} - R_{\mathrm{feed-in}} + C_{\mathrm{netw}} \tag{1}$$

The annualized equipment costs consist of annualized investments as well as annual operation and maintenance costs, both expressed by a fix proportion of the investment:

$$C_{\mathrm{EH}} = \sum_{k \in \mathrm{K_{EH}}} \left(C_{\mathrm{inv},k} + C_{\mathrm{om},k} \right) \tag{2}$$

$$= \sum_{k \in \mathrm{K_{EH}}} I_{k,\mathrm{EH}} \left(a_{\mathrm{inv},k} + f_{\mathrm{om},k} \right) \tag{3}$$

Here, the set of all available technologies in the energy hub is denoted by K_{EH}. The factor $a_{\mathrm{inv},k}$ denotes the capital recovery factor for each technology and $f_{\mathrm{om},k}$ denotes the share for operation and maintenance costs. All cost parameters are listed in Appendix A.2. Accordingly, the equipment costs

for the BES of all buildings $b \in B$ are:

$$C_{\mathrm{BES}} = \sum_{b \in \mathrm{B}} \sum_{k \in \mathrm{K_{BES}}} I_{k,b} \left(a_{\mathrm{inv},k} + f_{\mathrm{om},k} \right) \tag{4}$$

The investment for technology k is modeled with constant specific investments i:

$$I_{k,\mathrm{EH}} = i_{k,\mathrm{EH}} \; cap_{k,\mathrm{EH}} \quad \forall \; k \in \mathrm{K_{EH}} \tag{5}$$

$$I_{k,b} = i_{k,\mathrm{BES}} \; cap_{k,b} \quad \forall \; k \in \mathrm{K_{BES}}, \quad b \in \mathrm{B} \tag{6}$$

Here, cap_k denotes the rated power of each component k. For heating and cooling units, this is the rated heating and cooling power, for power generating units (CHP, PV), it is the rated electrical power. For energy storages, cap_k represents the storage capacity.

The gas costs consist of two components: energy supply costs for the total amount of gas purchased (G_{grid}) and capacity costs for the rated capacity of the gas connection ($\dot{G}_{\mathrm{grid}}^{\mathrm{nom}}$):

$$C_{\mathrm{gas}} = G_{\mathrm{grid}} \; p_{\mathrm{gas}}^{\mathrm{work}} + \dot{G}_{\mathrm{grid}}^{\mathrm{nom}} \; p_{\mathrm{gas}}^{\mathrm{cap}} \tag{7}$$

Here, $p_{\mathrm{gas}}^{\mathrm{work}}$ denotes the energy supply price (EUR/MWh) and $p_{\mathrm{gas}}^{\mathrm{cap}}$ the capacity price (EUR/MW). The total gas demand of the system is obtained by adding up the gas demand over all time steps t of all design days d:

$$G_{\mathrm{grid,tot}} = \sum_{d \in \mathrm{D}} w_d \sum_{t \in \mathrm{T}} \left(\dot{G}_{\mathrm{BOI,EH},d,t} + \dot{G}_{\mathrm{CHP,EH},d,t} \right) \Delta t \tag{8}$$

Here, Δt denotes the duration of the time steps and w_d are weighting factors for each design day which indicate how many days of the year are represented

by a particular design day. The capacity of the gas connection ($\dot{G}_{\text{grid}}^{\text{nom}}$) must be equal (or greater) than the peak gas demand during the year:

$$\dot{G}_{\text{BOI,EH},d,t} + \dot{G}_{\text{CHP,EH},d,t} \leq \dot{G}_{\text{grid}}^{\text{nom}} \quad \forall \;\; d \in \text{D}, \;\; t \in \text{T} \tag{9}$$

Similar to the gas costs, the electricity costs consist of energy supply costs ($p_{\text{el},d,t}^{\text{work}}$) and capacity costs ($p_{\text{el}}^{\text{cap}}$):

$$C_{\text{el}} = \sum_{d \in \text{D}} w_d \sum_{t \in \text{T}} P_{\text{grid},d,t} \; p_{\text{el},d,t}^{\text{work}} \Delta t + P_{\text{grid}}^{\text{nom}} \; p_{\text{el}}^{\text{cap}} \tag{10}$$

The supply price ($p_{\text{el},d,t}^{\text{work}}$) varies in time and is based on historical EPEX SPOT price data (c.f. Appendix A.3). The grid connection ($P_{\text{grid}}^{\text{nom}}$) must be equal (or larger) than the electric power purchased ($P_{\text{grid},d,t}$) or fed-in ($P_{\text{feed-in},d,t}$) for every single time step:

$$P_{\text{grid},d,t} \leq P_{\text{grid}}^{\text{nom}} \quad \forall \;\; d \in \text{D}, \;\; t \in \text{T} \tag{11}$$

$$P_{\text{feed-in},d,t} \leq P_{\text{grid}}^{\text{nom}} \quad \forall \;\; d \in \text{D}, \;\; t \in \text{T} \tag{12}$$

In the superstructure, two power generation technologies are available: CHP units and photovoltaic modules (PV). Thus, feed-in revenues amount to

$$R_{\text{feed-in}} = R_{\text{feed-in,CHP}} + R_{\text{feed-in,PV}} \tag{13}$$

The feed-in revenue of each technology results from the feed-in power and the specific feed-in revenue ($r_{\text{feed-in},k,d,t}$):

$$R_{\text{feed-in,CHP}} = \sum_{d \in \text{D}} w_d \sum_{t \in \text{T}} \left(P_{\text{feed-in,CHP},d,t} \; r_{\text{feed-in,CHP},d,t} \right) \Delta t \tag{14}$$

$$R_{\text{feed-in,PV}} = \sum_{d \in \text{D}} w_d \sum_{t \in \text{T}} \left(P_{\text{feed-in,PV},d,t} \; r_{\text{feed-in,PV},d,t} \right) \Delta t \tag{15}$$

q The annualized costs comprise installation costs for pipes and hydraulic pumps and are calculated a priori. They are a constant offset in the objective function and are not affected by the optimal solution. However, the annualized network costs are considered in order to achieve a valid cost comparison with a reference system (without thermal network) in the case study. The calculation of the network costs is elaborated in Appendix A.4.

2.1.2. Building energy system

In this section, the constraints for the technologies in the building energy systems are presented. The superstructure of the building energy systems is illustrated in Fig. 2. For heat generation, a heat pump (HP) can be installed. The heat source of the heat pump is the warm pipe of the BLTN. For peak loads, an electric boiler (EB) and a thermal energy storage (TES) is available. For the cooling supply, a compression chiller (CC) can be installed which uses the cold pipe of the BLTN as heat sink. If the temperatures of the cold network line are sufficiently low, direct cooling (DRC) with a heat exchanger that thermally connects the BLTN with the cooling circuit of the building can take place. Furthermore, a cooling tower (CT) which dissipates heat to the environment can be installed. Its operation depends on the ambient air temperature.

Generation units

The thermal output of all components must not exceed its rated power:

$$\dot{Q}_{\mathrm{h},k,b,d,t} \leq \dot{Q}^{\mathrm{nom}}_{\mathrm{h},k,b} \quad \forall\, k \in \{\mathrm{HP}, \mathrm{EB}\}, \quad b \in \mathrm{B}, \quad d \in \mathrm{D}, \quad t \in \mathrm{T} \tag{16}$$

$$\dot{Q}_{\mathrm{c},k,b,d,t} \leq \dot{Q}^{\mathrm{nom}}_{\mathrm{c},k,b} \quad \forall\, k \in \{\mathrm{CC}, \mathrm{DRC}, \mathrm{CT}\}, \quad b \in \mathrm{B}, \quad d \in \mathrm{D}, \quad t \in \mathrm{T} \tag{17}$$

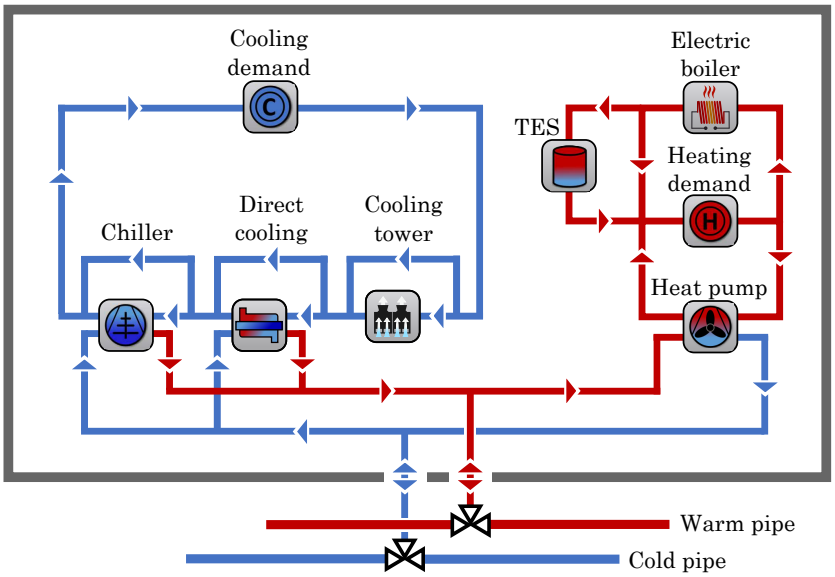

Figure 2: Superstructure of the building energy system. Heating demands are covered by heat pump, electric boiler and thermal energy storage (TES). Cooling demands are covered by compression chiller, heat exchanger (direct cooling) or cooling tower.

Here, $\dot{Q}^{\text{nom}}_{\text{h},k,b}/\dot{Q}^{\text{nom}}_{\text{c},k,b}$ denotes the rated heating/cooling power of the component k in building b and $\dot{Q}_{\text{h},k,b,d,t}/\dot{Q}_{\text{c},k,b,d,t}$ the heating/cooling output at time step t of design day d. The thermal output of heat pumps, electric boilers and compression chillers is expressed with their thermal efficiencies:

$$\dot{Q}_{\text{h,HP},b,d,t} = P_{\text{HP},b,d,t}\ COP_{\text{HP},b,d,t} \quad \forall\ b \in \text{B},\quad d \in \text{D},\quad t \in \text{T} \tag{18}$$

$$\dot{Q}_{\text{h,EB},b,d,t} = P_{\text{EB},b,d,t}\ \eta_{\text{EB}} \quad \forall\ b \in \text{B},\quad d \in \text{D},\quad t \in \text{T} \tag{19}$$

$$\dot{Q}_{\text{c,CC},b,d,t} = P_{\text{CC},b,d,t}\ COP_{\text{CC},b,d,t} \quad \forall\ b \in \text{B},\quad d \in \text{D},\quad t \in \text{T} \tag{20}$$

For electric boilers, a constant thermal efficiency is assumed. The coefficient of performance (COP) of the heat pumps and compression chillers are calculated based on a thermodynamic model presented by Jensen et al. [42]. All relevant model parameters are listed in Appendix A.1.

Energy storages

All thermal storages are water storages and modeled as ideally mixed. The state of charge increases linearly with the mean temperature of the storage fluid. The capacity of the hot water storage in building b is denoted by $S^{\mathrm{cap}}_{\mathrm{TES},b}$ and limited by an upper bound $S^{\mathrm{cap,max}}_{\mathrm{TES},b}$. This bound results from limited installation space in the buildings:

$$S^{\mathrm{cap}}_{\mathrm{TES},b} \leq S^{\mathrm{cap,max}}_{\mathrm{TES},b} \quad \forall\ b \in \mathrm{B} \tag{21}$$

The state of charge $S_{\mathrm{TES},b,d,t}$ must not exceed the nominal storage capacity:

$$S_{\mathrm{TES},b,d,t} \leq S^{\mathrm{cap}}_{\mathrm{TES},b} \quad \forall\ b \in \mathrm{B},\quad d \in \mathrm{D},\quad t \in \mathrm{T} \tag{22}$$

Charging the water storage is represented by heat flow $\dot{Q}^{\mathrm{ch}}_{\mathrm{h,TES},b}$, discharging by $\dot{Q}^{\mathrm{dch}}_{\mathrm{h,TES},b}$. Charging and discharging efficiencies ($\eta^{\mathrm{ch}}_{\mathrm{TES}}/\eta^{\mathrm{dch}}_{\mathrm{TES}}$) as well as heat losses ($\phi_{\mathrm{TES,loss}}$) are taken into account. The state of charge for all time steps $t > 1$ is:

$$\begin{aligned} S_{\mathrm{TES},b,d,t} = {} & S_{\mathrm{TES},b,d,t-1}(1 - \phi_{\mathrm{TES,loss}}) \\ & + \eta^{\mathrm{ch}}_{\mathrm{TES}} \dot{Q}^{\mathrm{ch}}_{\mathrm{h,TES},b,d,t} - \frac{\dot{Q}^{\mathrm{dch}}_{\mathrm{h,TES},b,d,t}}{\eta^{\mathrm{dch}}_{\mathrm{TES}}} \\ & \forall\ b \in \mathrm{B},\quad d \in \mathrm{D},\quad t \in \mathrm{T} \end{aligned} \tag{23}$$

The state of charge at the beginning of each day ($t = 1$), equals the state of charge at the end of the day (cyclic condition):

$$\begin{aligned} S_{\mathrm{TES},b,d,1} = {} & S_{\mathrm{TES},b,d,24}(1 - \phi_{\mathrm{TES,loss}}) \\ & + \eta^{\mathrm{ch}}_{\mathrm{TES}} \dot{Q}^{\mathrm{ch}}_{\mathrm{h,TES},b,d,1} - \frac{\dot{Q}^{\mathrm{dch}}_{\mathrm{h,TES},b,d,1}}{\eta^{\mathrm{dch}}_{\mathrm{TES}}} \\ & \forall\ b \in \mathrm{B},\quad d \in \mathrm{D} \end{aligned} \tag{24}$$

The state of charge of the first time step ($t = 1$) is identical for all design days:

$$S_{\mathrm{TES},b,d,1} = S^{\mathrm{init}}_{\mathrm{TES},b} \quad \forall\ b \in \mathrm{B} \tag{25}$$

In this formulation, the initial state of charge $S^{\mathrm{init}}_{\mathrm{TES},b}$ is a decision variable.

Energy balances

The heating and cooling demands of each building ($\dot{Q}_{\mathrm{h,dem},b,d,t}/\dot{Q}_{\mathrm{c,dem},b,d,t}$) is met by the BES:

$$\begin{aligned}&\dot{Q}_{\mathrm{h,HP},b,d,t} + \dot{Q}_{\mathrm{h,EB},b,d,t} + \dot{Q}^{\mathrm{dch}}_{\mathrm{h,TES},b,d,t} = \\ &\dot{Q}_{\mathrm{h,dem},b,d,t} + \dot{Q}^{\mathrm{ch}}_{\mathrm{h,TES},b,d,t} \quad \forall\ \ b \in \mathrm{B},\ \ d \in \mathrm{D},\ \ t \in \mathrm{T}\end{aligned} \tag{26}$$

The supply temperature of heat pumps equals the needed supply temperature of the heating circuit in the building (plus a temperature difference for the heat transfer). Since heat storages operate at temperatures above the supply temperature of the heating circuit, heat pumps cannot charge heat storages. As a result, heat storages can only be charged by electric boilers:

$$\dot{Q}_{\mathrm{h,EB},b,d,t} \geq \dot{Q}^{\mathrm{ch}}_{\mathrm{h,TES},b,d,t} \quad \forall\ \ b \in \mathrm{B},\ \ d \in \mathrm{D},\ \ t \in \mathrm{T} \tag{27}$$

On the cooling side, the cooling power of the compression chiller, direct cooler and cooling tower equals the cooling demand in each time step:

$$\dot{Q}_{\mathrm{c,CC},b,d,t} + \dot{Q}_{\mathrm{c,DRC},b,d,t} + \dot{Q}_{\mathrm{c,CT},b,d,t} = \dot{Q}_{\mathrm{c,dem},b,d,t} \quad \forall\ b \in \mathrm{B},\ \ d \in \mathrm{D},\ \ t \in \mathrm{T} \tag{28}$$

The electricity demand of the BES is

$$P_{\mathrm{BES},b,d,t} = P_{\mathrm{EB},b,d,t} + P_{\mathrm{HP},b,d,t} + P_{\mathrm{CC},b,d,t} \quad \forall\ \ b \in \mathrm{B},\ \ d \in \mathrm{D},\ \ t \in \mathrm{T} \tag{29}$$

and is met by the energy hub or the public electricity grid.

Cooling tower and direct cooler

At certain time steps (d, t), the operation of the cooling tower and direct cooler is restricted due to ambient air and network temperatures, respectively. In order to define for which time steps the cooling tower can be operated, the set

$$\Omega_{\mathrm{CT}} := \left\{(b, d, t) \in B \times D \times T \mid T_{\mathrm{air},d,t} + \Delta T_{\mathrm{CT}}^{\mathrm{min}} \leq T_{\mathrm{c,ret},b,d,t}\right\} \tag{30}$$

describes all combinations of buildings $b \in \mathrm{B}$, design days $d \in \mathrm{D}$ and time steps $t \in \mathrm{T}$ for which the ambient air temperature ($T_{\mathrm{air},d,t}$) is below the return temperature of the cooling circuit of the building ($T_{\mathrm{c,ret},b,d,t}$), plus a temperature difference for the heat transfer ($\Delta T_{\mathrm{CT}}^{\mathrm{min}}$). If the cooling tower can be operated, its cooling power ($\dot{Q}_{\mathrm{c,CT},b,d,t}$) is limited because it can cool the return line of the building's cooling circuit to a maximum of the ambient air temperature (plus $\Delta T_{\mathrm{CT}}^{\mathrm{min}}$):

$$\dot{Q}_{\mathrm{c,CT},b,d,t} \leq \frac{T_{\mathrm{c,ret},b,d,t} - \left(T_{\mathrm{air},d,t} + \Delta T_{\mathrm{CT}}^{\mathrm{min}}\right)}{T_{\mathrm{c,ret},b,d,t} - T_{\mathrm{c,sup},b,d,t}} \dot{Q}_{\mathrm{c,dem},b,d,t} \quad \forall\, (b, d, t) \in \Omega_{\mathrm{CT}} \tag{31}$$

$T_{\mathrm{c,sup},b,d,t}$ denotes the supply temperature of the building's cooling circuit. For all other combinations (b, d, t), the cooling tower cannot be operated:

$$\dot{Q}_{\mathrm{c,CT},b,d,t} = 0 \quad \forall\, (b, d, t) \notin \Omega_{\mathrm{CT}} \tag{32}$$

The direct cooler can only be operated if the fluid temperature in the warm pipe of the BLTN ($T_{\mathrm{h},d,t}^{\mathrm{netw}}$) is below the return temperature of the cooling circuit ($T_{\mathrm{c,ret},b,d,t}$). For defining the operational constraints of the direct cooler,

the set

$$\Omega_{\mathrm{DRC}} := \left\{(b,d,t) \in B \times D \times T \mid T^{\mathrm{netw}}_{\mathrm{h},d,t} + \Delta T^{\mathrm{min}}_{\mathrm{DRC}} \leq T_{\mathrm{c,ret},b,d,t}\right\} \tag{33}$$

is defined. Direct cooling is limited due to the maximum temperature drop it can achieve in the building's cooling circuit:

$$\dot{Q}_{\mathrm{c,DRC},b,d,t} \leq \frac{T_{\mathrm{c,ret},b,d,t} - \left(T^{\mathrm{netw}}_{\mathrm{c},d,t} + \Delta T^{\mathrm{min}}_{\mathrm{DRC}}\right)}{T_{\mathrm{c,ret},b,d,t} - T_{\mathrm{c,sup},b,d,t}} \dot{Q}_{\mathrm{c,dem},b,d,t} - \dot{Q}_{\mathrm{c,CT},b,d,t}$$
$$\forall\,(b,d,t) \in \Omega_{\mathrm{DRC}} \tag{34}$$

For combinations (b,d,t) for which the network temperature exceeds the return temperature of the cooling circuit, the direct cooler cannot be operated:

$$\dot{Q}_{\mathrm{c,DRC},b,d,t} = 0 \quad \forall\,(b,d,t) \notin \Omega_{\mathrm{DRC}} \tag{35}$$

As depicted in Fig. 2, the operation of the cooling tower affects direct cooling: Due to the operation of the cooling tower, the temperature of the return line can drop below the network temperature of the BLTN, which would disable direct cooling. To avoid this, the following constraint for the cooling tower is introduced:

$$\dot{Q}_{\mathrm{c,CT},b,d,t} \leq \frac{T_{\mathrm{c,ret},b,d,t} - \left(T^{\mathrm{netw}}_{\mathrm{h},d,t} + \Delta T^{\mathrm{min}}_{\mathrm{DRC}}\right)}{T_{\mathrm{c,ret},b,d,t} - T_{\mathrm{c,sup},b,d,t}} \dot{Q}_{\mathrm{c,dem},b,d,t} \quad \forall\,(b,d,t) \in \Omega_{\mathrm{DRC}} \tag{36}$$

Appendix B provides a detailed derivation of the operational constraints of cooling tower and direct cooler.

Peak load correction

Due to the design day clustering, peak heating and cooling demands can deviate from the unclustered annual time series. As a result, peak demands of

the clustered demand time series are smaller than the original peak demands. Smaller peak demands result in an undersizing of the equipment of the BES. In order ensure that peak demands of the unclustered time series can be met, the following constraints are formulated:

$$\dot{Q}^{\mathrm{peak}}_{\mathrm{h,HP},b} + \dot{Q}^{\mathrm{peak}}_{\mathrm{h,EB},b} = \dot{Q}^{\mathrm{peak}}_{\mathrm{h,dem},b} \quad \forall \;\; b \in \mathrm{B} \tag{37}$$

$$\dot{Q}^{\mathrm{peak}}_{\mathrm{c,CC},b} + \dot{Q}^{\mathrm{peak}}_{\mathrm{c,DRC},b} = \dot{Q}^{\mathrm{peak}}_{\mathrm{c,dem},b} \quad \forall \;\; b \in \mathrm{B} \tag{38}$$

Here, $\dot{Q}^{\mathrm{peak}}_{\mathrm{h,dem},b}$ and $\dot{Q}^{\mathrm{peak}}_{\mathrm{c,dem},b}$ denote the peak heating/cooling demands of the unclustered demand time series. The auxiliary variables $\dot{Q}^{\mathrm{peak}}_{\mathrm{h,HP},b}$ and $\dot{Q}^{\mathrm{peak}}_{\mathrm{h,EB},b}$ denote the heating power of the heat pump and electric boiler at the time step at which the peak heating demand occurs. Accordingly, the peak cooling demands are met by either the compression chiller or the direct cooler ($\dot{Q}^{\mathrm{peak}}_{\mathrm{c,CC},b}$ / $\dot{Q}^{\mathrm{peak}}_{\mathrm{c,DRC},b}$). The rated power of heating and cooling units ($\dot{Q}^{\mathrm{nom}}_{\mathrm{h},k,b}$/$\dot{Q}^{\mathrm{nom}}_{\mathrm{c},k,b}$) must be at least as high as the heating and cooling output during peak hours ($\dot{Q}^{\mathrm{peak}}_{\mathrm{h},k,b}$/$\dot{Q}^{\mathrm{peak}}_{\mathrm{c},k,b}$):

$$\dot{Q}^{\mathrm{peak}}_{\mathrm{h},k,b} \leq \dot{Q}^{\mathrm{nom}}_{\mathrm{h},k,b} \quad \forall \;\; k \in \{\mathrm{HP}, \mathrm{EB}\}, \quad b \in \mathrm{B} \tag{39}$$

$$\dot{Q}^{\mathrm{peak}}_{\mathrm{c},k,b} \leq \dot{Q}^{\mathrm{nom}}_{\mathrm{c},k,b} \quad \forall \;\; k \in \{\mathrm{CC}, \mathrm{DRC}\}, \quad b \in \mathrm{B} \tag{40}$$

The operation of direct coolers in each building depends on the network temperature of the BLTN at the time step of the building's peak cooling demand. If the network temperature is low enough for direct cooling, and the cooling power of the cooling tower is set to zero, from Eq. (34) follows

$$\dot{Q}^{\mathrm{peak}}_{\mathrm{c,DRC},b} \leq \frac{T^{\mathrm{peak}}_{\mathrm{c,ret},b} - \left(T^{\mathrm{netw,peak}}_{\mathrm{c},b} + \Delta T^{\mathrm{min}}_{\mathrm{DRC}}\right)}{T^{\mathrm{peak}}_{\mathrm{c,ret},b} - T^{\mathrm{peak}}_{\mathrm{c,sup},b}} \dot{Q}^{\mathrm{peak}}_{\mathrm{c,dem},b} \quad \forall \;\; b \in \Omega^{\mathrm{peak}}_{\mathrm{DRC}} \tag{41}$$

as limitation of the operation of direct coolers in the buildings. Here, the set

$$\Omega^{\mathrm{peak}}_{\mathrm{DRC}} := \left\{ b \in \mathrm{B} \mid T^{\mathrm{netw,peak}}_{\mathrm{h},b} + \Delta T^{\mathrm{min}}_{\mathrm{DRC}} \leq T^{\mathrm{peak}}_{\mathrm{c,ret},b} \right\} \tag{42}$$

contains all buildings which are able to use the direct cooler at the time step of their peak cooling demand. In other buildings, the direct cooler cannot be operated:

$$\dot{Q}^{\text{peak}}_{\text{c,DRC},b} = 0 \quad \forall \;\; b \notin \Omega^{\text{peak}}_{\text{DRC}} \tag{43}$$

2.1.3. Thermal network

The residual building demands that are met by the BLTN are:

$$\begin{aligned}\dot{Q}_{\text{res,BES},b,d,t} = \dot{Q}_{\text{h,HP},b,d,t} \left(1 - \frac{1}{COP_{\text{HP},b,d,t}}\right) \\ - \dot{Q}_{\text{c,CC},b,d,t} \left(1 + \frac{1}{COP_{\text{CC},b,d,t}}\right) \\ - \dot{Q}_{\text{c,DRC},b,d,t} \quad \forall \;\; b \in \text{B}, \;\; d \in \text{D}, \;\; t \in \text{T}\end{aligned} \tag{44}$$

Here, COP_{HP} and COP_{CC} denote the coefficient of performance of the heat pump and compression chiller, respectively. The residual thermal building demand ($\dot{Q}_{\text{res,BES},b,d,t}$) is a free variable and can take positive or negative values: Positive residual thermal demands mean a heat flow from the network to the building. Negative residual thermal demands indicate a heat flow from the building to the network. The energy hub covers the residual network load (including losses):

$$\dot{Q}_{\text{res,EH},d,t} = \sum_{b \in \text{B}} \dot{Q}_{\text{res,BES},b,d,t} + \dot{Q}_{\text{h,loss},d,t} - \dot{Q}_{\text{c,loss},d,t} + \dot{Q}_{\text{netw},d,t} \quad \forall \;\; d \in \text{D}, \;\; t \in \text{T} \tag{45}$$

$\dot{Q}_{\text{netw},d,t}$ denotes the internal energy needed to raise (or lower) the temperature of the network. It is calculated in a pre-processing step based on the water mass in the pipes and the (prescribed) network temperatures. If a constant network temperature is assumed, $\dot{Q}_{\text{netw},d,t}$ is zero. In this case, the sum

of all residual thermal building demands plus thermal network losses needs to be covered by the energy hub in order to maintain the network temperature. Since in Eq. (45) negative and positive residual thermal demands can be canceled out, this constraint also implies the balancing of demands in the BLTN. It is worth mentioning that this balancing process is assumed ideal, especially not constrained by hydraulic network limits. $\dot{Q}_{\mathrm{h,loss},d,t}/\dot{Q}_{\mathrm{c,loss},d,t}$ denote thermal losses of the warm and cold pipe of the BLTN and can take positive and negative values. The losses are calculated in a pre-processing step according to the following relations for the heat transfer from the network fluid to the surrounding soil:

$$\dot{Q}_{\mathrm{h,loss},d,t} = (kA)_{\mathrm{tot}} \left(T^{\mathrm{netw}}_{\mathrm{h},d,t} - T_{\mathrm{soil},d,t}\right) \quad \forall \;\; d \in \mathrm{D}, \;\; t \in \mathrm{T} \tag{46}$$

$$\dot{Q}_{\mathrm{c,loss},d,t} = (kA)_{\mathrm{tot}} \left(T_{\mathrm{soil},d,t} - T^{\mathrm{netw}}_{\mathrm{c},d,t}\right) \quad \forall \;\; d \in \mathrm{D}, \;\; t \in \mathrm{T} \tag{47}$$

$(kA)_{\mathrm{tot}}$ denotes the thermal transmittance including all heat transfer resistances from the fluid to the soil layer (with undisturbed soil temperature $T_{\mathrm{soil},d,t}$). Calculation details are given in Appendix A.4.

2.1.4. Energy hub

In this section, the constraints of the energy hub (EH) are presented. Fig. 3 shows the superstructure of the energy hub: For heat generation, a gas-fired and electric boiler (BOI/EB) as well as a gas-fired CHP unit is available. Cold is provided by a compression chiller (CC), absorption chiller (AC) and cooling tower (CT). The operation of the cooling tower depends on the ambient air temperature. In order to increase the flexibility of the system, a hot and a cold thermal energy storage (TES, CTES) as well as a battery (BAT) can be selected. Furthermore, PV modules can be installed.

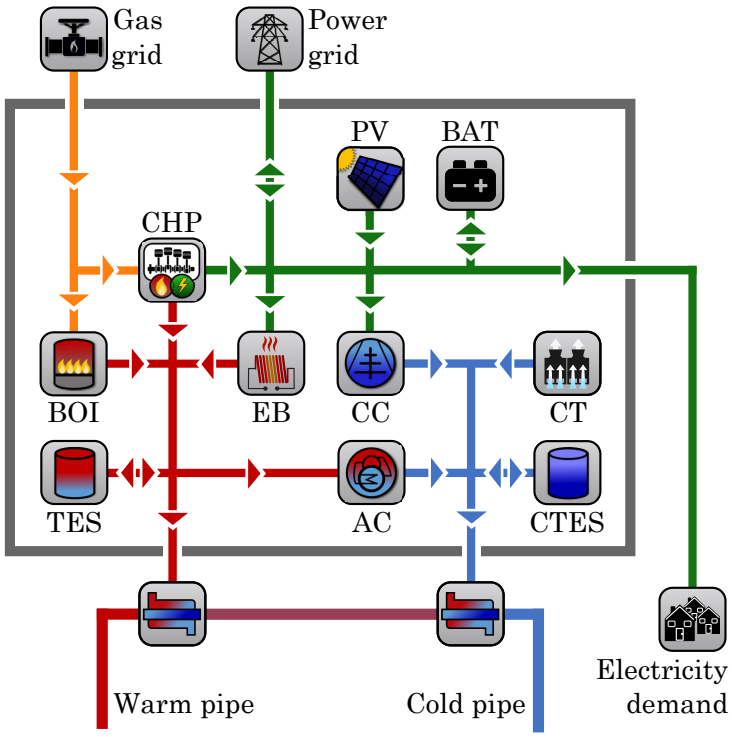

Figure 3: Superstructure of the energy hub: CHP unit, gas boiler (BOI) and electric boiler (EB) generate heat. Cold is generated by absorption chiller (AC), compression chiller (CC) and cooling tower (CT). Photovoltaic modules (PV) generate electricity. A heat storage (TES), cold storage (CTES) and battery (BAT) increase the operational flexibility.

A connection to the public power and gas grid is available. The energy hub provides heating and cooling power for the BLTN and covers electricity demands of the BESs.

Generation units

The thermal or electric power of the units is limited by their rated capacity:

$$\dot{Q}_{\mathrm{h},k,\mathrm{EH},d,t} \leq \dot{Q}^{\mathrm{nom}}_{\mathrm{h},k,\mathrm{EH}} \quad \forall\ k \in \{\mathrm{BOI}, \mathrm{EB}\}\,, \quad d \in \mathrm{D}, \quad t \in \mathrm{T} \tag{48}$$

$$\dot{Q}_{\mathrm{c},k,\mathrm{EH},d,t} \leq \dot{Q}^{\mathrm{nom}}_{\mathrm{c},k,\mathrm{EH}} \quad \forall\ k \in \{\mathrm{CC}, \mathrm{AC}, \mathrm{CT}\}\,, \quad d \in \mathrm{D}, \quad t \in \mathrm{T} \tag{49}$$

$$P_{k,\mathrm{EH},d,t} \leq P^{\mathrm{nom}}_{k,\mathrm{EH}} \quad \forall\ k \in \{\mathrm{CHP}, \mathrm{PV}\}\,, \quad d \in \mathrm{D}, \quad t \in \mathrm{T} \tag{50}$$

For PV modules, the module area (A_{PV}) determines the peak capacity. The total module area is limited by a maximum area ($A^{\mathrm{max}}_{\mathrm{PV}}$):

$$A_{\mathrm{PV}} \leq A^{\mathrm{max}}_{\mathrm{PV}} \tag{51}$$

For Standard Test Conditions (STC) [44], the rated power of the PV modules is

$$P^{\mathrm{nom}}_{\mathrm{PV}} = G_{\mathrm{sol,STC}} A_{\mathrm{PV}}\, \eta_{\mathrm{PV,STC}} \tag{52}$$

Here, $G_{\mathrm{sol,STC}}$ is the global tilted irradiance and $\eta_{\mathrm{PV,STC}}$ the electric efficiency under Standard Test Conditions. The gas boiler and the electric boiler is modeled with constant thermal efficiencies:

$$\dot{Q}_{\mathrm{h,BOI,EH},d,t} = \dot{G}_{\mathrm{BOI,EH},d,t}\, \eta_{\mathrm{BOI}} \quad \forall\ \ d \in \mathrm{D}, \quad t \in \mathrm{T} \tag{53}$$

$$\dot{Q}_{\mathrm{h,EB,EH},d,t} = P_{\mathrm{EB,EH},d,t}\, \eta_{\mathrm{EB}} \quad \forall\ \ d \in \mathrm{D}, \quad t \in \mathrm{T} \tag{54}$$

The compression chiller is modeled with a time-dependent COP and the absorption chiller with a constant heat ratio β_{AC}:

$$\dot{Q}_{\mathrm{c,CC,EH},d,t} = P_{\mathrm{CC,EH},d,t}\, COP_{\mathrm{CC},d,t} \quad \forall\ \ d \in \mathrm{D}, \quad t \in \mathrm{T} \tag{55}$$

$$\dot{Q}_{\mathrm{c,AC,EH},d,t} = \dot{Q}_{\mathrm{h,AC,EH},d,t}\, \beta_{\mathrm{AC}} \quad \forall\ \ d \in \mathrm{D}, \quad t \in \mathrm{T} \tag{56}$$

Here, $\dot{Q}_{\mathrm{h,AC,EH},d,t}$ denotes the heat flow that drives the AC, and $\dot{Q}_{\mathrm{c,AC,EH},d,t}$ the cooling power provided by the AC. Constant thermal and electric effi-

ciencies are used for the CHP unit:

$$P_{\mathrm{CHP,EH},d,t} = \dot{G}_{\mathrm{CHP,EH},d,t}\, \eta_{\mathrm{el,CHP}} \quad \forall \;\; d \in \mathrm{D}, \;\; t \in \mathrm{T} \tag{57}$$

$$\dot{Q}_{\mathrm{h,CHP,EH},d,t} = \dot{G}_{\mathrm{CHP,EH},d,t}\, \eta_{\mathrm{th,CHP}} \quad \forall \;\; d \in \mathrm{D}, \;\; t \in \mathrm{T} \tag{58}$$

The power of the PV modules is constrained by the power that can be generated based on the global tilted irradiance ($G_{\mathrm{sol},d,t}$) and the module efficiency ($\eta_{\mathrm{PV},d,t}$).

$$P_{\mathrm{PV},d,t} \leq G_{\mathrm{sol},d,t} A_{\mathrm{PV}}\, \eta_{\mathrm{PV},d,t} \quad \forall \;\; d \in \mathrm{D}, \;\; t \in \mathrm{T} \tag{59}$$

The inequality constraint enables curtailment of PV power.

Energy storages

For modeling energy storages in the energy hub, a modeling approach presented by Gabrielli et al. [45] and Kotzur et al. [46] is used. Based on the design day clustering, each design day d can be assigned to one of the 365 days of the original annual time series. The set of all original days is denoted by $Y = \{1, 2, ..., 365\}$. The assignment between the original days $y \in \mathrm{Y}$ and the design days $d \in \mathrm{D}$ is denoted by σ:

$$\sigma : Y \rightarrow D,\, \sigma(y) = d \tag{60}$$

If σ is evaluated for all days y, the order of the used design days during the course of the year is obtained. This allows considering decision variables which cannot reasonably modeled when using design days, such as the state of charge of storages in the EH. To enable a seasonal storage operation, the state of charge has to be modeled for each day y of the year.

The state of charge at time step t is connected to the state of charge of the previous time step $(t-1)$ considering charging and discharging efficiencies as well as thermal losses, yielding

$$\begin{aligned} S_{k,\mathrm{EH,y,t}} = {} & S_{k,\mathrm{EH,y,t-1}} \left(1 - \phi_{k,\mathrm{EH,loss}}\right) \\ & + \eta^{\mathrm{ch}}_{k,\mathrm{EH}} P^{\mathrm{ch}}_{k,\mathrm{EH},\sigma(y),t} - \frac{P^{\mathrm{dch}}_{k,\mathrm{EH},\sigma(y),t}}{\eta^{\mathrm{dch}}_{k,\mathrm{EH}}} \\ & \forall \;\; k \in \{\mathrm{TES}, \mathrm{CTES}, \mathrm{BAT}\}, \quad y \in \mathrm{Y}, \quad t \in \mathrm{T} \setminus \{1\} \end{aligned} \tag{61}$$

Here, $P^{\mathrm{ch}}/P^{\mathrm{dch}}$ denote generalized energy flows to charge or discharge the storage. In case of the TES or CTES, they represent $\dot{Q}^{\mathrm{ch}}_{\mathrm{h}}/\dot{Q}^{\mathrm{dch}}_{\mathrm{h}}$ or $\dot{Q}^{\mathrm{ch}}_{\mathrm{c}}/\dot{Q}^{\mathrm{dch}}_{\mathrm{c}}$, respectively.

In order to model the transition between two consecutive days, the first time step of the day y is connected to the 24th time step of the previous day $(y-1)$:

$$\begin{aligned} S_{k,\mathrm{EH,y,1}} = {} & S_{k,\mathrm{EH,y-1,24}} \left(1 - \phi_{k,\mathrm{EH,loss}}\right) \\ & + \eta^{\mathrm{ch}}_{k,\mathrm{EH}} P^{\mathrm{ch}}_{k,\mathrm{EH},\sigma(y),1} - \frac{P^{\mathrm{dch}}_{k,\mathrm{EH},\sigma(y),1}}{\eta^{\mathrm{dch}}_{k,\mathrm{EH}}} \\ & \forall \;\; k \in \{\mathrm{TES}, \mathrm{CTES}, \mathrm{BAT}\}, \quad y \in \mathrm{Y} \setminus \{1\} \end{aligned} \tag{62}$$

The cyclic condition connects the first time step of the first day with the 24th time step of the 365th day:

$$\begin{aligned} S_{k,\mathrm{EH},1,1} = {} & S_{k,\mathrm{EH},365,24} \left(1 - \phi_{k,\mathrm{EH,loss}}\right) \\ & + \eta^{\mathrm{ch}}_{k,\mathrm{EH}} P^{\mathrm{ch}}_{k,\mathrm{EH},\sigma(1),1} - \frac{P^{\mathrm{dch}}_{k,\mathrm{EH},\sigma(1),1}}{\eta^{\mathrm{dch}}_{k,\mathrm{EH}}} \\ & \forall \;\; k \in \{\mathrm{TES}, \mathrm{CTES}, \mathrm{BAT}\} \end{aligned} \tag{63}$$

The storage capacity is limited by an upper bound:

$$S_{k,\mathrm{EH}}^{\mathrm{cap}} \leq S_{k,\mathrm{EH}}^{\mathrm{cap,max}} \quad \forall \;\; k \in \{\mathrm{TES}, \mathrm{CTES}, \mathrm{BAT}\} \tag{64}$$

Additionally, the state of charge is bound within a minimum and maximum proportion of the rated storage capacity ($s_k^{\mathrm{min}}/s_k^{\mathrm{max}}$):

$$S_{k,\mathrm{EH},y,t} \leq s_k^{\mathrm{max}} S_{k,\mathrm{EH}}^{\mathrm{cap}} \quad \forall \;\; k \in \{\mathrm{TES}, \mathrm{CTES}, \mathrm{BAT}\}, \quad y \in \mathrm{Y}, \quad t \in \mathrm{T} \tag{65}$$

$$S_{k,\mathrm{EH},y,t} \geq s_k^{\mathrm{min}} S_{k,\mathrm{EH}}^{\mathrm{cap}} \quad \forall \;\; k \in \{\mathrm{TES}, \mathrm{CTES}, \mathrm{BAT}\}, \quad y \in \mathrm{Y}, \quad t \in \mathrm{T} \tag{66}$$

The maximum charging and discharging power is limited by a minimal charging and discharging time τ, respectively:

$$P_{\mathrm{k,EH,d,t}}^{\mathrm{ch}} \leq \frac{S_{k,\mathrm{EH}}^{\mathrm{cap}}}{\tau_k} \quad \forall \;\; k \in \{\mathrm{TES}, \mathrm{CTES}, \mathrm{BAT}\}, \quad d \in \mathrm{D}, \quad t \in \mathrm{T} \tag{67}$$

$$P_{\mathrm{k,EH,d,t}}^{\mathrm{dch}} \leq \frac{S_{k,\mathrm{EH}}^{\mathrm{cap}}}{\tau_k} \quad \forall \;\; k \in \{\mathrm{TES}, \mathrm{CTES}, \mathrm{BAT}\}, \quad d \in \mathrm{D}, \quad t \in \mathrm{T} \tag{68}$$

Heat and cold storages in the energy hub are assumed ideally mixed. The temperature range for both is given in Table A.7.

Energy balances

In order to balance residual loads of the BLTN, the energy hub heats or cools the network. As described in Eq. (45), residual heating and cooling demands that have to be balanced by the energy hub are aggregated in the decision variable $\dot{Q}_{\mathrm{res,EH},d,t}$, which can be positive (residual heating demand) or negative (residual cooling demand). Therefore, only one energy balance

for heating and cooling is formulated:

$$\begin{aligned}
&\dot{Q}_{\mathrm{h,BOI,EH},d,t} + \dot{Q}_{\mathrm{h,CHP,EH},d,t} + \dot{Q}_{\mathrm{h,EB,EH},d,t} + \dot{Q}^{\mathrm{dch}}_{\mathrm{h,TES,EH},d,t} \\
&- \dot{Q}_{\mathrm{c,CC,EH},d,t} - \dot{Q}_{\mathrm{c,AC,EH},d,t} - \dot{Q}_{\mathrm{c,CT,EH},d,t} - \dot{Q}^{\mathrm{dch}}_{\mathrm{c,CTES,EH},d,t} = \\
&\dot{Q}_{\mathrm{res,EH},d,t} + \dot{Q}_{\mathrm{h,AC,EH},d,t} + \dot{Q}^{\mathrm{ch}}_{\mathrm{h,TES,EH},d,t} - \dot{Q}^{\mathrm{ch}}_{\mathrm{c,CTES,EH},d,t} \\
&\forall \;\; d \in \mathrm{D}, \quad t \in \mathrm{T}
\end{aligned} \tag{69}$$

To avoid violating the second law of thermodynamics, two additional constraints are introduced: Firstly, the absorption chiller as well as the thermal energy storage are only supplied with heat from the gas boiler, electric boiler or CHP unit. If this constraint is omitted, it would be possible to cover residual cooling demands by charging the heat storage. This is not possible since the temperature level of the heat storage is always higher than the network temperature.

$$\begin{aligned}
&\dot{Q}_{\mathrm{h,BOI,EH},d,t} + \dot{Q}_{\mathrm{h,CHP,EH},d,t} + \dot{Q}_{\mathrm{h,EB,EH},d,t} \geq \\
&\dot{Q}_{\mathrm{h,AC,EH},d,t} + \dot{Q}^{\mathrm{ch}}_{\mathrm{h,TES,EH},d,t} \quad \forall \;\; d \in \mathrm{D}, \quad t \in \mathrm{T}
\end{aligned} \tag{70}$$

Likewise, the cold storage can only be charged by the compression or absorption chiller:

$$\dot{Q}_{\mathrm{c,CC,EH},d,t} + \dot{Q}_{\mathrm{c,AC,EH},d,t} \geq \dot{Q}^{\mathrm{ch}}_{\mathrm{c,CTES,EH},d,t} \quad \forall \;\; d \in \mathrm{D}, \quad t \in \mathrm{T} \tag{71}$$

The operation of the cooling tower in the energy hub depends on the ambient air temperature. As stated above, the cooling tower cannot charge the cold storage. Thus, it can only contribute to the cooling power transferred from the energy hub to the network, which is given by

$$\begin{aligned}
\dot{Q}^{\mathrm{netw}}_{\mathrm{c,EH},d,t} = {} & \dot{Q}_{\mathrm{c,CC,EH},d,t} + \dot{Q}_{\mathrm{c,AC,EH},d,t} + \dot{Q}_{\mathrm{c,CT,EH},d,t} \\
& + \dot{Q}^{\mathrm{dch}}_{\mathrm{c,CTES,EH},d,t} - \dot{Q}^{\mathrm{ch}}_{\mathrm{c,CTES,EH},d,t} \quad \forall \;\; d \in \mathrm{D}, \quad t \in \mathrm{T}
\end{aligned} \tag{72}$$

To identify time steps at which the air temperature is low enough for the cooling tower to operate, the set

$$\Lambda_{\mathrm{CT}} := \left\{ (d,t) \in D \times T \mid T_{\mathrm{air},d,t} + \Delta T_{\mathrm{CT}}^{\mathrm{min}} \leq T_{\mathrm{h},d,t}^{\mathrm{netw}} \right\} \tag{73}$$

is introduced. The cooling power of the cooling tower is then constrained by

$$\dot{Q}_{\mathrm{c,CT,EH},d,t} \leq \frac{T_{\mathrm{h},d,t}^{\mathrm{netw}} - \left(T_{\mathrm{air},d,t} + \Delta T_{\mathrm{CT}}^{\mathrm{min}} \right)}{T_{\mathrm{h},d,t}^{\mathrm{netw}} - T_{\mathrm{c},d,t}^{\mathrm{netw}}} \dot{Q}_{\mathrm{c,EH},d,t}^{\mathrm{netw}} \quad \forall\, (d,t) \in \Lambda_{\mathrm{CT}} \tag{74}$$

If the air temperature is too high, the cooling tower cannot be operated:

$$\dot{Q}_{\mathrm{c,CT,EH},d,t} = 0 \quad \forall\, (d,t) \notin \Lambda_{\mathrm{CT}} \tag{75}$$

Besides a connection to the public power grid $P_{\mathrm{grid},d,t}$, the CHP unit and the PV modules ($P_{\mathrm{CHP,EH},d,t}/P_{\mathrm{PV},d,t}$) as well as discharging the battery ($P_{\mathrm{BAT,EH},d,t}^{\mathrm{dch}}$) can contribute to cover the electricity demands:

$$\begin{aligned} & P_{\mathrm{CHP,EH},d,t} + P_{\mathrm{PV},d,t} + P_{\mathrm{grid},d,t} + P_{\mathrm{BAT,EH},d,t}^{\mathrm{dch}} = \\ & \sum_{b \in B} P_{\mathrm{BES},b,d,t} + P_{\mathrm{EB,EH},d,t} + P_{\mathrm{CC,EH},d,t} + P_{\mathrm{feed-in},d,t} \\ & + P_{\mathrm{BAT,EH},d,t}^{\mathrm{ch}} + P_{\mathrm{pumps},d,t} \quad \forall \;\; d \in \mathrm{D}, \;\; t \in \mathrm{T} \end{aligned} \tag{76}$$

The electricity demands on the right hand side result from the electricity demands of the BESs ($\sum_{b \in B} P_{\mathrm{BES},b,d,t}$), electric boiler and compression chiller in the energy hub ($P_{\mathrm{EB,EH},d,t}/P_{\mathrm{CC,EH},d,t}$), the feed-in power to the public power grid ($P_{\mathrm{feed-in},d,t}$), the charging power of the battery ($P_{\mathrm{BAT},d,t}^{\mathrm{ch}}$) and the electricity demand of the hydraulic pumps of the network. The electric demands of the hydraulic pumps is calculated in a pre-processing step as elaborated in Appendix A.4.

Due to different feed-in rates in the German power market for CHP power and PV power, the feed-in power is split:

$$P_{\text{feed-in},d,t} = P_{\text{feed-in,CHP},d,t} + P_{\text{feed-in,PV},d,t} \quad \forall \ \text{d} \in D, \quad t \in \text{T} \tag{77}$$

The feed-in power is limited by the generated power of its technology for each time step. Electric power from the battery can be fed-in as well. Since the feed-in revenue rate for CHP power is lower than for PV power, it is assumed that the feed-in revenue rate for battery power equals the revenue rate for CHP power. This is expressed by

$$P_{\text{feed-in,CHP},d,t} \leq P_{\text{CHP,EH},d,t} + P^{\text{dch}}_{\text{BAT,EH},d,t} \quad \forall \ d \in \text{D}, \quad t \in \text{T} \tag{78}$$

$$P_{\text{feed-in,PV},d,t} \leq P_{\text{PV},d,t} \quad \forall \ d \in \text{D}, \quad t \in \text{T} \tag{79}$$

The total number of decision variables N of the Linear Program can be approximated with the number of buildings connected to the BLTN (N_{B}) and the number of design days (N_{D}):

$$N = (2500 + 480 N_{\text{B}})\, N_{\text{D}} \tag{80}$$

2.2. Model limitations

In this section, the most important simplifications and assumptions of the Linear Program are highlighted. In particular, the thermal network and the operation of the energy conversion units are modeled in a simplified way:

- A global energy balance for the entire BLTN is formulated (Eq. 69). This energy balance has to be satisfied for all time steps. If more thermal energy is taken by the buildings from the network than injected, it is assumed that the energy hub covers these residual demands perfectly

and, as a result, network temperatures remain constant. The validity of this assumption depends on the network topology, size and the operation strategy of the network itself [47]. Nonetheless, the two most relevant losses, hydraulic and thermal losses, are considered: Based on prescribed network temperatures, thermal losses (or gains) from the fluid to the surrounding are calculated a priori and considered in the model (Eq. (45)). Likewise, pump work is calculated in a pre-processing step (c.f. Appendix A.4) and considered in the power balance of the energy hub (Eq. (76)).

- The operation of all energy conversion units is modeled in a simplified manner. In contrast to more detailed MILP formulations, minimum part-load limitations ([48], [49]), part-load efficiencies of the components ([50], [51]), minimum rated capacities [52], non-linear investment curves [53] and ramping constraints ([54], [55]) are neglected. Furthermore, a predefined temperature lift of heat pumps are assumed, i.e. the operating temperature levels of heat pumps are not optimized: Heat pumps in buildings raise the temperature just to the supply temperature of the heating circuit in the building.

- Although a comprehensive technology choice is modeled for the superstructure of the LP, the following technologies are not considered: Reversible heat pumps are not part of the superstructure of the building energy system. They can be profitable if direct cooling with the network is not possible and heating and cooling demands do not occur at the same time. Furthermore, geothermal borehole fields are

not considered, which can be used as heating or cooling source for the BLTN or, depending on the ground conditions, as long-term storages (e.g. aquifer storage). Besides PV, other renewable technologies, such as wind turbines or solar thermal collectors, are not considered. Different storage technologies, like ice storages are not part of the model. No hydrogen-based technologies, such as electrolyzers or fuel cells, are considered.

- No power losses or line limits are considered for the electrical network.

2.3. Performance indicators

In this section, key figures to evaluate the performance of the energy system are introduced.

Economic indicators

The objective function of the LP (TAC) is an economic performance indicator. The specific costs for covering the total heating and cooling demands in the district ($Q_{\mathrm{h,dem,tot}}/Q_{\mathrm{c,dem,tot}}$) are

$$c_{\mathrm{tot}} = \frac{TAC}{Q_{\mathrm{h,dem,tot}} + Q_{\mathrm{c,dem,tot}}} \tag{81}$$

Thermodynamic indicators

In order to evaluate the energetic performance of an energy system, the ratio of useful energy to the total energetic expenditure is considered. Based on a concept presented by Rosen et al. [56], a *figure of merit* is defined as:

$$f = \frac{Q_{\mathrm{h,dem,tot}} + Q_{\mathrm{c,dem,tot}} + W_{\mathrm{feed-in,tot}}}{G_{\mathrm{grid,tot}} + W_{\mathrm{grid,tot}} + W_{\mathrm{PV,tot}}} \tag{82}$$

The useful energy consists of the total annual heating and cooling demand of all buildings and the total electricity fed into the grid ($W_{\mathrm{feed-in,tot}}$). The total amounts of gas ($G_{\mathrm{grid,tot}}$) and electricity ($W_{\mathrm{grid,tot}}$) taken from the respective grid are considered as expenditures. For photovoltaics, only the proportion that is actually converted into electrical energy is considered as expenditure ($W_{\mathrm{PV,tot}}$). Due to the equal weight for different forms of energy, this figure can be larger than 1. In order to take into account the thermodynamic quality of different forms of energy, the exergy efficiency is evaluated as:

$$\eta_{\mathrm{ex}} = \frac{E_{\mathrm{h,dem,tot}} + E_{\mathrm{c,dem,tot}} + W_{\mathrm{feed-in,tot}}}{R_{\mathrm{gas}} G_{\mathrm{grid,tot}} + W_{\mathrm{grid,tot}} + W_{\mathrm{PV,tot}} + E_{\mathrm{CT,tot}}} \tag{83}$$

Here, the reference temperature is $T_{\mathrm{ref}} = 25\,^{\circ}\mathrm{C} = 298.15\,\mathrm{K}$. For the exergy of natural gas, an energy grade function of $R_{\mathrm{gas}} = 0.913$ is taken into account [56]. The definition of the exergy grade of cold flows is based on Jansen et al. [57]. To evaluate the exergy of the heating and cooling demands, the corresponding supply temperatures $T_{\mathrm{h,sup}}$ and $T_{\mathrm{c,sup}}$ of the building circuits are used:

$$E_{\mathrm{h,dem,tot}} = \sum_{\mathrm{b}\in\mathrm{B}} \sum_{d\in\mathrm{D}} w_d \sum_{t\in\mathrm{T}} \dot{Q}_{\mathrm{h,dem},b,d,t} \left(1 - \frac{T_{\mathrm{ref}}}{T_{\mathrm{h,sup},b,d,t}}\right) \Delta t \tag{84}$$

$$E_{\mathrm{c,dem,tot}} = \sum_{b\in\mathrm{B}} \sum_{d\in\mathrm{D}} w_d \sum_{t\in\mathrm{T}} \dot{Q}_{\mathrm{c,dem},b,d,t} \left(\frac{T_{\mathrm{ref}}}{T_{\mathrm{c,sup},b,d,t}} - 1\right) \Delta t \tag{85}$$

$E_{\mathrm{CT,tot}}$ denotes the exergy transferred to the system by cooling towers. Cooling towers provide useful exergy (a share of $E_{\mathrm{c,dem,tot}}$) without causing an expenditure. If this portion is neglected, systems with large cooling tower contributions could achieve exergy efficiencies greater than 1. Based on Jansen

et al. [57], the exergy provided by cooling towers is

$$E_{\mathrm{CT,tot}} = \sum_{b\in\mathrm{B}} \sum_{d\in\mathrm{D}} w_d \sum_{t\in\mathrm{T}} \dot{Q}_{\mathrm{c,CT},b,d,t} \left(\frac{T_{\mathrm{ref}}}{T_{\mathrm{c,sup},b,d,t}} - 1 \right) \Delta t + \sum_{d\in\mathrm{D}} w_d \sum_{t\in\mathrm{T}} \dot{Q}_{\mathrm{c,CT,EH},d,t} \left(\frac{T_{\mathrm{ref}}}{T^{\mathrm{netw}}_{\mathrm{c},d,t}} - 1 \right) \Delta t \tag{86}$$

Environmental indicators

For evaluating the environmental impact, the emitted carbon dioxide emissions and the primary energy factor are calculated. The specific CO_2 emissions are

$$e_{\mathrm{tot}} = \frac{e_{\mathrm{gas}} G_{\mathrm{grid,tot}} + e_{\mathrm{el}} \left(W_{\mathrm{grid,tot}} - W_{\mathrm{feed-in,tot}} \right)}{Q_{\mathrm{h,dem,tot}} + Q_{\mathrm{c,dem,tot}}} \tag{87}$$

Here, e_{gas} and e_{el} denote the specific CO_2 emissions of burning natural gas and the electricity taken from the grid, respectively. The electricity fed into the grid is considered as avoided burden.

Similarly, the primary energy factor is evaluated by

$$PEF_{\mathrm{tot}} = \frac{PEF_{\mathrm{gas}} G_{\mathrm{grid,tot}} + PEF_{\mathrm{el}} \left(W_{\mathrm{grid,tot}} - W_{\mathrm{feed-in,tot}} \right)}{Q_{\mathrm{h,dem,tot}} + Q_{\mathrm{c,dem,tot}}} \tag{88}$$

Here, PEF_{gas} and PEF_{el} denote the primary energy factors of natural gas and electricity taken from the grid, respectively. All specific emissions and primary energy factors are listed in Appendix A.5.

3. Case study

In this section, all relevant technical details of the use case are described. The results of the case study are presented in Section 4.

3.1. Use case description

The LP formulation is applied to a research campus in Germany. Currently, all buildings of the campus are supplied by district heating and cooling networks. In the past, a monitoring system has been installed, which comprises smart meters at the substation of each building. The smart meters log heating and cooling consumption with an sub-hourly time resolution. Raw data was aggregated to annual time series with an hourly time resolution. The resulting heating and cooling time series of 17 buildings are used as input data in this study. The total heating and cooling demands of all buildings are depicted for one year in Fig. 4. The annual heating demand is 6.36 GWh with a peak demand of 2.01 MW. The annual cooling demand is 10.04 GWh and shows a peak of 2.42 MW. The building stock comprises laboratories, office buildings as well as two data centers. The geographical arrangement of the buildings together with their heating and cooling demand is illustrated in Fig. 5. Building 3 and 4 are data centers which cause 73 % of the district's cooling demand. Buildings 10, 11, 16 and 17 are office buildings, in which thermal demands result from space heating and cooling. Laboratory buildings are 5, 8, 12, 14 and 15. In these buildings, a substantial proportion of demands results from process heat and cold for experiments. Buildings 6, 7, 9 and 13 have a mixed utilization (office and laboratories). Building 2 is a canteen, which has a large heating load due to process heat. The supply temperature of the heating circuits in the buildings is assumed 60 °C, the return temperature 30 °C. For covering the cooling demands in the buildings, a cooling supply temperature of 16 °C with a return temperature of 20 °C is assumed. For the cooling circuits in the data centers, a cooling return

temperature of 30 °C is assumed. All supply and return temperatures are assumed constant throughout the year.

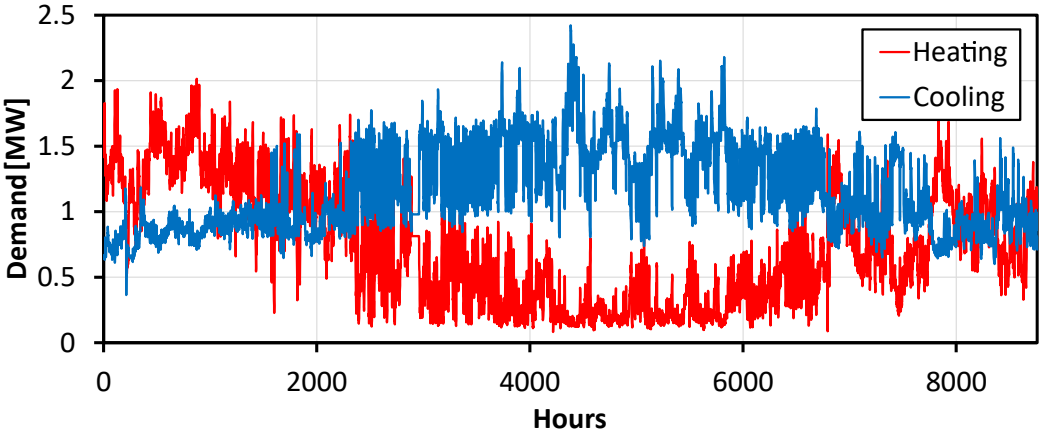

Figure 4: Cumulated heating and cooling demands of all buildings for one year.

The demand time series are clustered to 50 design days. The LP formulation for 17 buildings comprises 530,000 decision variables. The computation time for one optimization run is approx. 30 seconds (Intel Core i5-7200U CPU). The Linear Program is set up in *Python* and solved using the solver *Gurobi 7.5.1*.

3.2. Supply scenarios

In order to evaluate the performance of the BLTN, an alternative supply scenario in which all buildings are equipped with individual HVAC systems (no thermal network present) is considered. Both supply scenarios (BLTN and individual supply) are described in the following.

3.2.1. Bidirectional low temperature network

In this scenario, all buildings of the district are connected to a BLTN. The fluid temperature in the warm pipe is assumed $T_{\mathrm{h}}^{\mathrm{netw}} = 18$ °C and in

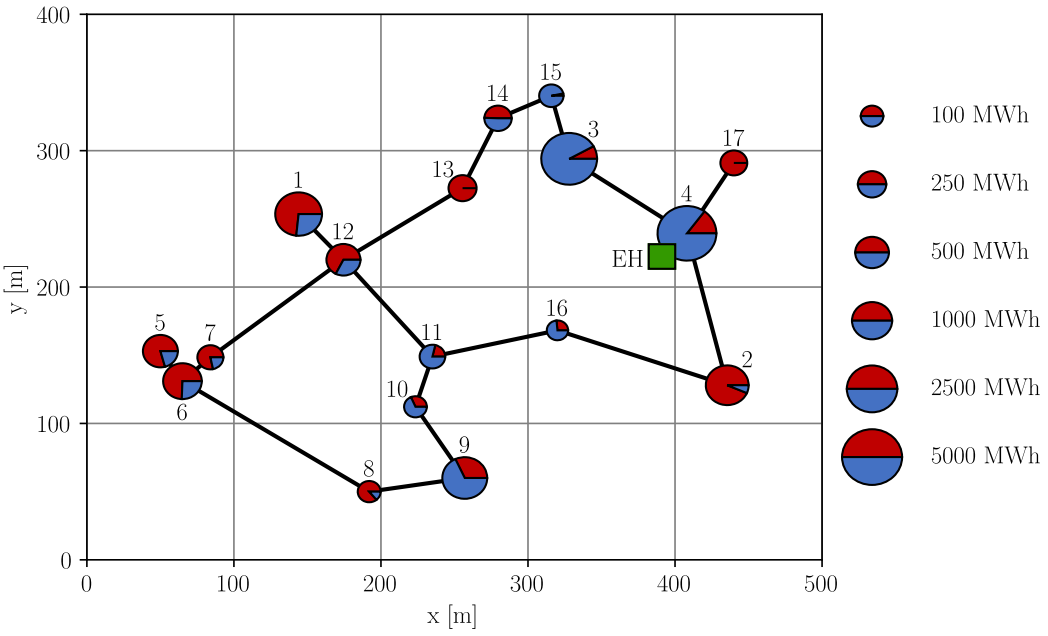

Figure 5: Geographical arrangement of the 17 buildings with their annual heating (red) and cooling demands (blue). Furthermore, the network topology of the BLTN and the location of the energy hub (EH), which have been determined prior to the optimization, are illustrated.

the cold pipe $T_{\mathrm{c}}^{\mathrm{netw}} = 14\ ^{\circ}\mathrm{C}$. The network temperatures are assumed constant throughout the year. The low temperatures enable direct cooling in all buildings. Based on the network temperature and supply temperature in the buildings, the COP of the heat pumps is 5.05. Compression chillers connected to the BLTN reach a COP of 6. The storage capacity of the heat and cold storages are limited by an assumed maximum volume $V_{\max}$:

$$S_{k,\mathrm{EH}}^{\mathrm{cap,max}} = \rho_{\mathrm{w}} V_{\max} c_{\mathrm{p,w}} \left(T_{k,\max} - T_{k,\min}\right) \quad \forall\ k \in \{\mathrm{TES}, \mathrm{CTES}\} \tag{89}$$

Here, ρ_{w} and $c_{\mathrm{p,w}}$ denote the density ($1000\ \frac{\mathrm{kg}}{\mathrm{m}^3}$) and heat capacity ($4.18\ \frac{\mathrm{kJ}}{\mathrm{kg\,K}}$) of water, respectively. The maximum storage volumes and capacities of the

storages in the buildings and the energy hub are listed in Appendix A.1. The capacity of the battery is limited by $S^{\text{cap,max}}_{\text{BAT,EH}} = 10\,\text{MWh}$ and the PV area by $A^{\text{max}}_{\text{PV}} = 5000\,\text{m}^2$.

3.2.2. Stand-alone HVAC systems

In this supply scenario, individual HVAC systems are designed for each building without considering a BLTN or energy hub. This scenario serves as benchmark for the BLTN scenario. The superstructure of the HVAC systems comprise air source heat pumps, electric boilers and thermal energy storages for covering heating demands. Compression chillers and cooling towers are available for covering cooling demands. The COP calculation of the air source heat pumps and compression chillers is based on Jensen et al. [42], the model parameter are listed in Appendix A.1. The COP of the air source heat pumps range between 2.34 and 4.60 over the year and the COP of the compression chillers between 3.05 and 6. As in the BLTN scenario, for PV modules an area of $A^{\text{max}}_{\text{PV}} = 5000\,\text{m}^2$ is available. PV power can be exchanged among buildings without losses or limitations.

4. Results

In this section, the results of the case study for the two supply scenarios introduced in the previous section are presented.

4.1. Cost structure

For the BLTN scenario, the specific energy supply costs are 22.61 EUR/MWh ($TAC = 371\,\text{kEUR/a}$). The specific costs in the stand-alone supply scenario are substantially larger (38.66 EUR/MWh, $TAC = 634\,\text{kEUR/a}$).

The cost portions for both scenarios are depicted in Fig. 6. The share "electricity" includes costs for purchasing electricity from the public grid (energy supply price) as well as costs for the peak power (capacity price). In the BLTN solution, the electricity costs are 18.9 kEUR/a (5 % of TAC). In the stand-alone supply scenario, the electricity costs are the largest cost portion (421.3 kEUR/a, 66 % of TAC) since only electrically driven technologies are available (heat pumps, chillers and electric boilers). The electricity must be purchased from the public power grid or is provided by PV modules. Revenues from electricity feed-in are 51.9 kEUR/a in the BLTN scenario and 16.4 kEUR/a in the stand-alone supply scenario. In the BLTN scenario, almost the entire electric power generated by the CHP unit or PV modules is consumed on-site (98 %).

Like the electricity costs, the gas costs include energy supply costs (for the gas amount) and capacity costs (for the grid connection). The gas costs in the BLTN scenario are 130.8 kEUR/a (35 % of TAC).

In the BLTN scenario, the annualized investments for the components in the energy hub (EH) are 147.2 kEUR/a (40 % of TAC) and for the components of the BESs 94.1 kEUR/a (25 % of TAC). In the stand-alone supply scenario, the annualized investments for the BESs are 144.8 kEUR/a (23 % of TAC). Since the only technology available in the EH is PV, the EH costs of 84.5 kEUR/a (13 % of TAC) are the costs for PV modules.

The annualized costs for the network (pipe material, groundworks and hydraulic pumps) account for 31.7 kEUR/a (9 % of TAC). The calculation of the network costs is described in Appendix A.4. For the stand-alone supply scenario, no thermal network is installed ($C_{\mathrm{netw}} = 0$).

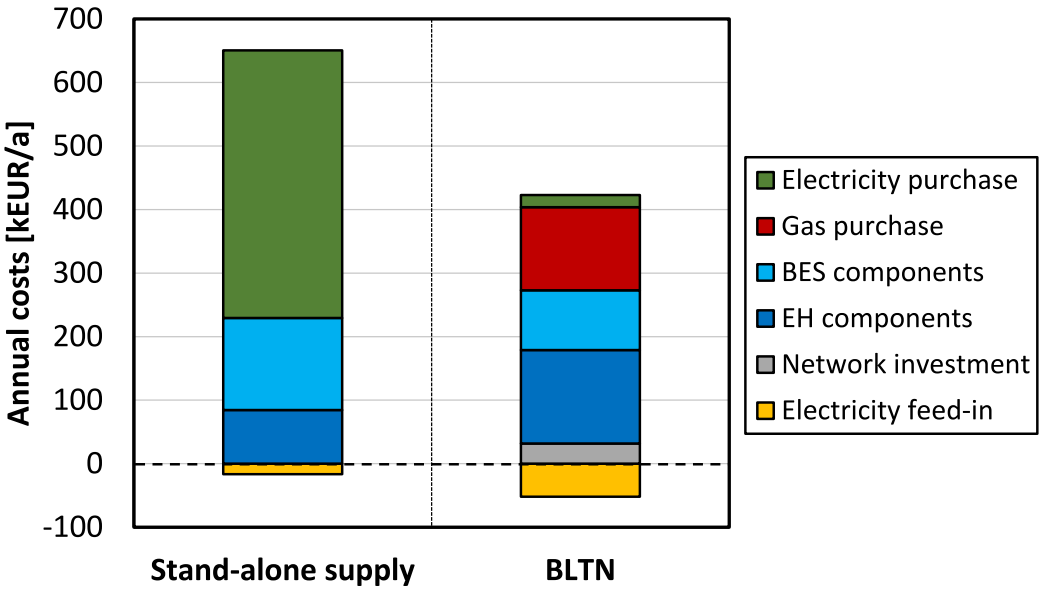

Figure 6: Cost comparison between BLTN scenario and stand-alone supply scenario.

4.2. Installed capacities and generation

The rated capacities as well as the heating, cooling and electricity generation of all technologies in the EH are listed in Table 1. For gas boilers, the rated capacity refers to the rated heat output, for CHP units and PV modules it refers to the rated electric power and for compression and absorption chillers as well as cooling towers the rated power refers to the rated cooling power. Peak heat demands are met by a gas boiler with a rated thermal power of 0.22 MW. The gas boiler is only operated at peak times, which results in low full load hours (351 $\frac{\text{h}}{\text{a}}$). In addition, a CHP unit with a capacity of 0.26 MW is installed (full load hours: 6733 $\frac{\text{h}}{\text{a}}$). The cooling load is covered by a compression and absorption chiller (2.04 MW/0.16 MW). The absorption chiller shows high full load hours (4283 $\frac{\text{h}}{\text{a}}$) and is mainly driven by heat from the CHP unit. Neither electric boilers nor cooling towers are installed

in the EH. The installed PV peak power is 0.63 MW which equals a module area of 3034 m^2 (61 % of available installation area). In the stand-alone supply scenario, the maximum feasible PV capacity is installed (1.04 MW, 5000 m^2).

Table 1: Installed capacity and operation of components in energy hub.

Technology	Capacity	Generation	Full load hours $\left[\frac{h}{a}\right]$
Gas boiler	0.22 MW_{th}	77 MWh_{th}	351
CHP unit	0.26 MW_{el}	1750 MWh_{el}	6733
El. boiler	—	—	—
Comp. chiller	2.04 MW_{th}	3250 MWh_{th}	1593
Abs. chiller	0.16 MW_{th}	685 MWh_{th}	4283
Cooling tower	—	—	—
PV	0.63 MW_{peak}	701 MWh_{el}	1113

The superstructure of the EH comprises three different storage types: a heat and cold storage as well as a battery. The optimal solution contains a heat storage with a capacity of 1.72 MWh. Based on the temperature range of the heat storage (20 – 90 °C), this equals a water volume of 21.16 m^3. Furthermore, a cold storage with a capacity of 0.48 MWh is selected, which equals a water volume of 41.34 m^3 (temperature range 2 – 12 °C). Despite the smaller storage capacity, the investments for the cold storage are about twice the investments for the heat storage. The optimal energy system does not contain a battery. In Fig. 7, the state of charge of the thermal storages in the EH are depicted. In winter, the heat storage is operated with short cycle times in order to buffer peak heat demands. In summer, residual heat

demands occur less frequently and are less prominent. Thus, the usage of the heat storage is much less frequently and larger cycle times are observed. The cold storage is operated with short cycle times throughout the year. The more frequent charging and discharging of the cold storage appears reasonable considering the higher investments compared to the heat storage.

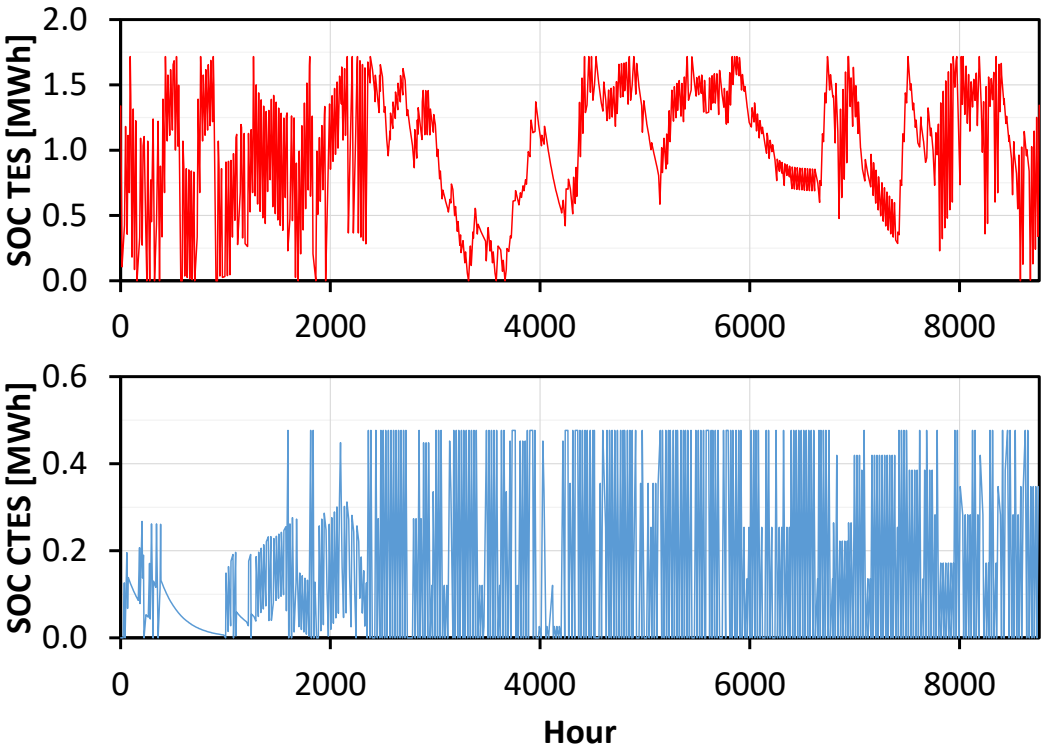

Figure 7: State of charge (SOC) of heat and cold storages in the energy hub.

The capacity of the connection to the public power grid is 0.21 MW. The power exchange with the power grid is depicted in Fig. 8 as sorted annual load curve. The grid connection is mainly used for power feed-in (black line) and only during peak hours, power is taken from the public grid (red line).

The cumulated installed capacities in the BESs are displayed in Table 2.

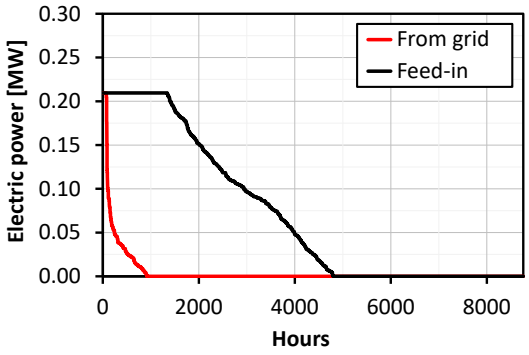

Figure 8: Sorted annual load curve of electric power from the public grid (red) and feed-in power to the public grid (black). The capacity of the grid connection is 0.21 MW.

In total, 1.82 MW capacity of heat pumps and 0.58 MW capacity of electric boilers are installed. Electric boilers cover peak heat demands (full load hours: $60\,\frac{\mathrm{h}}{\mathrm{a}}$) and provide 35 MWh of heat (0.6 % of the total heat demand). Despite their very limited operation, they enable to reduce the heat pump capacity in the buildings. Thus, due to their lower specific investments (150 EUR/kW) compared to heat pumps (300 EUR/kW), they reduce the total investments for the BESs. In 16 of 17 buildings, heat storages are installed. The total storage capacity is 0.34 MWh. Heat storages are used to cover peak heat demands in winter. Cooling demands are covered by direct coolers and cooling towers. Since the network temperatures enable direct cooling, no compression chillers are needed. Cooling towers are only installed in the data centers.

In Fig. 9, the balancing of thermal demands is depicted. Fig. 9a shows the heating and cooling demands. The deviations from Fig. 4 result from the design days clustering. Fig. 9b shows the heating and cooling demands which are not balanced within the BESs (intra-building balancing). The remaining

Table 2: Cumulated installed capacity and operation of components in building energy systems.

Technology	Capacity	Generation	Full load hours $\left[\frac{\mathrm{h}}{\mathrm{a}}\right]$
Heat pump	$1.82\,\mathrm{MW_{th}}$	$6331\,\mathrm{MWh_{th}}$	3478
Electric boiler	$0.58\,\mathrm{MW_{el}}$	$35\,\mathrm{MWh_{el}}$	60
Comp. chiller	—	—	—
Direct cooler	$2.86\,\mathrm{MW_{th}}$	$8160\,\mathrm{MWh_{th}}$	2853
Cooling tower	$0.46\,\mathrm{MW_{th}}$	$1882\,\mathrm{MWh_{th}}$	4090

building demands are covered by the BLTN. If the remaining heating and cooling demands of different buildings overlap, they can be partially balanced within the BLTN (one building supplies another with waste heat). The demands which are not balanced in the BLTN are covered by the EH. These residual demands are displayed in Fig. 9c. The demand balancing substantially reduces the heating demands. However, the peak cooling demands in summer remain almost on the same level, which causes a large chiller capacity in the EH.

4.3. Thermodynamic and environmental performance indicators

In this section, the thermodynamic and environmental performance indicators as introduced in Section 2.3 are evaluated. In the BLTN scenario, the figure of merit (FOM) is 3.40 and the exergy efficiency 34.1 %. In comparison, the FOM in the stand-alone supply scenario is larger (4.36), however the exergy efficiency is lower (30.2 %). The large FOM in the stand-alone supply scenario results from the fact that predominantly heat pumps and chillers are used which themself achieve a large FOM, i.e. COP. In the BLTN scenario,

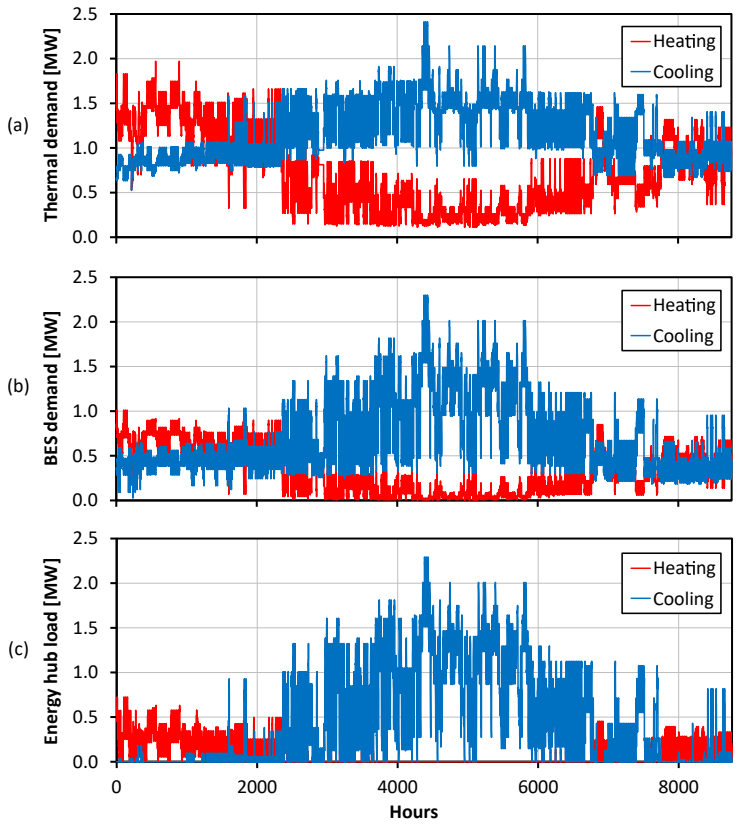

Figure 9: a) Cumulated heating and cooling demands. b) Remaining thermal demands which are not balanced within BESs. c) Residual thermal demands which are not balanced within the BLTN and, therefore, must be met by the energy hub.

a substantial amount of end energy is natural gas. If natural gas is used by a gas boiler or CHP unit for heating the BLTN, almost all exergy is lost due to the low network temperatures in the warm pipe (18 °C). In the buildings, the temperature level must then be increased by heat pumps again. From an exergetic point of view, heating the network with gas-fired technologies is not beneficial.

In the BLTN, the total annual CO_2 emissions are 559 t/a. This equals

specific CO_2 emissions of 34.1 kg/MWh (referred to the total heating and cooling demand). The stand-alone supply scenario causes substantially more emissions (1266 t/a; 77.2 kg/MWh). However, in the stand-alone supply scenario, the emissions strongly depend on the electricity mix of the public power grid since all end energy is electricity. The primary energy demand in the BLTN scenario is 3650 MWh, which equals a primary energy factor of 0.22. In the stand-alone supply scenario, the primary energy demand is 4418 MWh and the primary energy factor 0.27.

4.4. Exemplary operation of the BLTN

In this section, the operation of the BLTN for two example days is described: one cold winter and one hot summer day.

4.4.1. Summer day

On this day, the cooling demand of the buildings is covered by direct cooling and in the data centers to some extent by cooling towers. Heating demands are covered by heat pumps only. The operation of the EH is depicted in Fig. 10. The three illustrations show the heat, cold and electricity flows to and from each component. The operation of heat, cold or electricity generators is illustrated as stacked areas. The thermal and electrical demands are displayed as stacked lines. For a valid energy balance (supply equals demand), the topmost line (demand) and the upper edge of the topmost area (supply) lie on top of each other. As depicted in the top illustration, the residual cooling demand is covered by the compression chiller (CC) and absorption chiller (AC). Between 4:00 and 10:00, cooling power of the AC is used to charge the cold storage. By discharging the cold storage, this excess

cooling power is then used to cover peak residual cooling demands between 16:00 and 20:00. The AC is driven by heat from the CHP unit (as depicted in the heat balance). Moreover, the CHP unit covers a small residual heat demand ($< 0.1\,\mathrm{MW}$) which occurs between 4:00 and 9:00 in the morning. In the evening hours (16:00 – 21:00) the heat storage is charged with excess heat.

On this day, the aggregated power demand of the BESs (black line in the illustration of the electricity balance) ranges between 0.05 and 0.2 MW. The power demand of the BESs and the compression chiller (blue line) in the EH, are covered by the CHP unit and PV power. During noon hours, excess power is fed into the public power grid. Due to the large generation of PV power during noon hours, the cooling power of the AC is reduced and the operation of compression chiller is increased.

4.4.2. Winter day

In Fig. 11, the operation of the EH during a winter day is displayed. Due to the large heat demands in buildings and the operation of the heat pumps, a large residual heat demand has to be covered by the EH. The residual heat demand is covered by the gas boiler, CHP unit and heat storage. The CHP unit is operated at full load during the entire day. The boiler is operated at full load during the morning hours. In order to cover peak heat demands, the heat storage is discharged during the morning. In the evening hours, the storage is charged. The operation of the CHP unit also covers a large proportion of the electrical demands which mainly result from the operation of the heat pumps and electric boilers in the buildings. The remaining power demands are covered by PV during noon hours and, especially during the

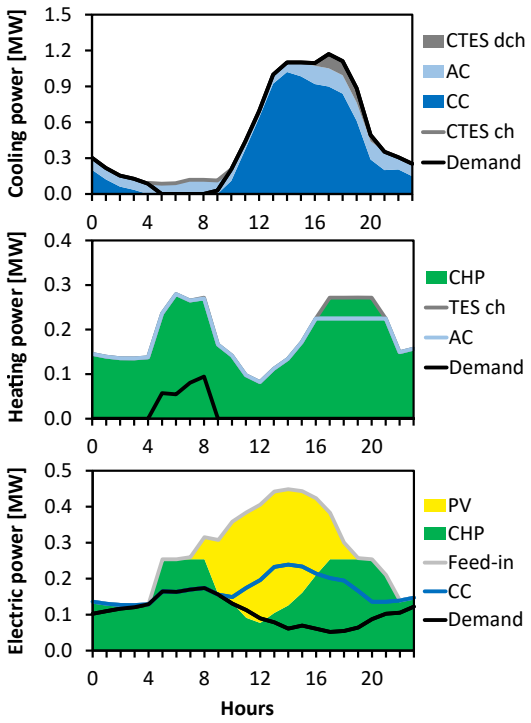

Figure 10: Operation of energy hub on a summer day.

morning hours, by power from the public electricity grid.

The operation of the BESs is shown in Fig. 12. Here, the aggregated heating demands and the total heat generation in all 17 buildings are depicted. The main proportion of the heat demand is covered by heat pumps (HP). During morning hours, electric boilers (EB) are operated. They cover peak heat demands and, during the night, they charge the heat storages in the buildings. In order to cover the peak heat demand between 6:00 and 9:00, the heat storages are discharged. This day demonstrates that the operation of electric boilers can be useful although most of the electricity is taken from the public grid.

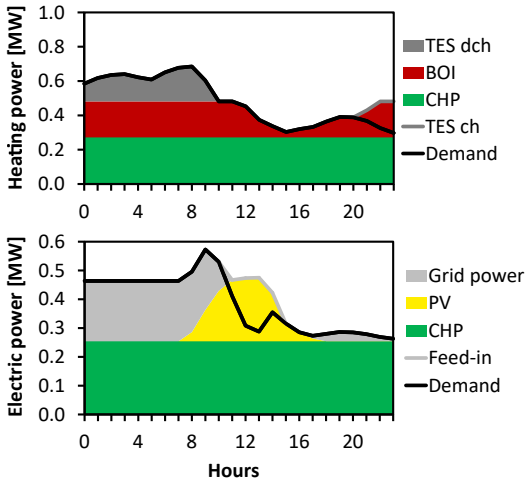

Figure 11: Operation of energy hub on a winter day.

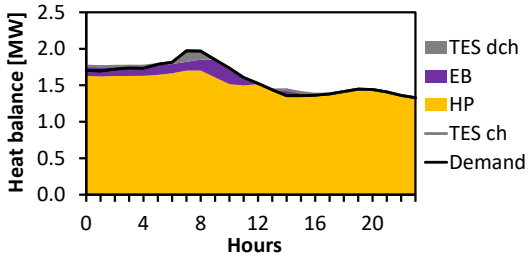

Figure 12: Operation of heat generating units aggregated for all 17 buildings.

5. Conclusions and outlook

5.1. Conclusions

Bidirectional low temperature networks (BLTN) are an efficient technology to recover local waste heat in urban districts. Due to the mutual heat exchange between buildings, holistic design methodologies which consider the district energy system as a whole are necessary. A Linear Program for designing BLTNs is presented and applied to a real-world use case. The performance of the BLTN is compared to a heating and cooling supply with

individual HVAC systems. The BLTN leads to substantially less total annualized costs (−42 %), causes less CO_2 emissions (−56 %) and has a larger exergy efficiency (34.1 % compared to 30.2 %). However, the results cannot simply be generalized to other districts as the performance of the BLTN depends strongly on the available local waste heat potential.

In the case study, heat pumps are installed to cover heating demands in buildings. Peak heating demands are met by electric boilers and heat storages in buildings. It appears profitable to operate the network at temperatures which enable direct cooling in buildings. Then, no compression chillers have to be installed, which would result in larger investments. In the data centers, cooling towers dissipate excess heat directly to the environment which is advantageous when waste heat cannot be reused by other buildings, e.g. in summer.

For the energy hub, the installation of a trigeneration system with CHP unit, compression and absorption chiller as well as a gas boiler for peak demands is optimal. Heat and cold storages are an optimal supplement, as they increase the operation flexibility of the generation units.

The exemplary operation of the BLTN on two example days clearly shows the need for advanced design approaches. The high interaction of all system components makes the design process more complex. For example, it does not always make sense to feed all available waste heat into the BLTN. Instead, it can be advantageous for the overall system to install cooling towers, and thus enable to dissipate waste heat to the environment. Therefore, this study also shows the need for holistic design approaches for BLTNs in order to achieve an optimal interaction of all components of the system.

5.2. Outlook

In future work, the presented Linear Program can be enhanced in different ways in order to increase its applicability. It is assumed that all buildings are connected to the BTLN. However, this assumption might not be valid for other use cases and can lead to a sub-optimal system design. In order to determine the optimal set of buildings that should be connected to the BLTN, binary variables have to be introduced.

In order to enhance the model, further energy conversion technologies can be added to the superstructure, e.g. a geothermal borehole field or an (reversible) air source heat pump in the energy hub. Furthermore, solar thermal collectors can be considered for building roofs. Innovative storage technologies such as ice storages or large seasonal storages can also be integrated.

In the presented use case, constant operating network temperatures are assumed. However, the model also allows to prescribe variable operating network temperatures over the year. In future work, the model can be used to determine an optimal temperature curve over the year.

6. Acknowledgments

This work was supported by the Helmholtz Association under the Joint Initiative "Energy System 2050 – A Contribution of the Research Field Energy".

We would also like to thank Helen Carlström, part of the ectogrid^{TM} team at E.ON, for the fruitful collaboration while carrying out this research study.

7. Nomenclature

Abbreviations

AC	Absorption Chiller
BAT	Battery
BES	Building Energy System
BLTN	Bidirectional Low Temperature Network
BOI	Gas Boiler
CC	Compression Chiller
CHP	Combined Heat and Power
CT	Cooling Tower
CTES	Cold Thermal Energy Storage
DHC	District Heating and Cooling
EB	Electric Boiler
EH	Energy Hub
FOM	Figure of Merit
DRC	Direct Cooler
HP	Heat Pump
HVAC	Heating, Ventilation and Air Conditioning
LP	Linear Program
MILP	Mixed-Integer Linear Program
PV	Photovoltaics
SOC	State of Charge
STC	Standard Test Conditions
TAC	Total Annualized Costs
TES	Thermal Energy Storage

Indices and Sets

$b \in \mathrm{B}$ Buildings

$d \in \mathrm{D}$ Design days

$t \in \mathrm{T}$ Time steps

$y \in \mathrm{Y}$ Days of the year

Variables

A Roof area

cap Device capacity

C Annualized costs

E Exergy

G Gas energy

I Investment

P Electric power

Q Thermal energy

R Annualized revenue

S State of charge

W Electric energy

Parameters

β	Heat ratio
η	Efficiency
ρ	Density
$\sigma(y)$	Design day assignment function
ϕ_{loss}	Loss factor
τ	Minimum charging/discharging time
a_{inv}	Capital recovery factor
c	Specific costs
c_{p}	Specific heat capacity
e	Specific CO_2 emissions
COP	Coefficient of performance
f	Figure of merit
f_{om}	Cost share for operation & maintenance
i	Specific investments
kA	Thermal transmittance
N	Number of decision variables
p	Specific price
PEF	Primary energy factor
r	Specific revenue
R_{gas}	Energy grade function of natural gas
s	Proportion of storage capacity
T	Temperature
V	Storage volume
w_d	Design day weight

Sub- and Superscripts

el	electric
ex	exergy
c	cooling
cap	capacity
ch	charge
dch	discharge
dem	demand
h	heating
init	initial
max	maximum
min	minimum
netw	network
nom	nominal
sol	solar
sup	supply
ref	reference
res	residual
ret	return
th	thermal
tot	total
w	water

Appendix A. Model parameters

Appendix A.1. Technical parameters

The heat pump and compression chiller COPs are calculated based on a model by Jensen et al. [42]. The isentropic efficiency of the compressor $\eta_{\mathrm{is,c}}$, the compressor heat losses f_{Q} and the pinch point temperature difference ΔT_{pp} are given in Table A.3. The refrigerant is assumed ammonia. The COP is limited by 7 for heat pumps (HP) and 6 for compression chillers (CC). For HPs and CCs used in the stand-alone HVAC scenario, a temperature difference of 10 K between air and refrigerant is assumed.

Table A.3: Parameters for COP calculation.

	$\eta_{\mathrm{is,c}}$ [-]	f_{Q} [-]	ΔT_{pp} [K]
HP	0.8	0.1	2
CC	0.75	0.1	2

For PV, the electrical efficiency depends on the ambient temperature and solar radiation and is calculated based on [58]. PV module data is based on the module LG360Q1C-A5 [59] which shows a conversion efficiency of $\eta_{\mathrm{PV,STC}} = 0.208$ under Standard Test Conditions.

Efficiencies of generation units are listed in Table A.4. Technical parameters of storage technologies are listed in Table A.5. Minimum temperature differences for the operation of the direct coolers and cooling towers are listed in Table A.6. The maximum storage capacities assumed in the case study are given in Table A.7.

Table A.4: Constant conversion efficiencies (EH and BES).

η_{BOI} [−]	$\eta_{\mathrm{el,CHP}}$ [−]	$\eta_{\mathrm{th,CHP}}$ [−]	β_{AC} [−]	η_{EB} [−]
0.90	0.419	0.448	0.68	0.95

Table A.5: Technical storage parameters (EH and BES).

	η^{ch} [−]	η^{dch} [−]	ϕ_{loss} [−]	τ [h]	s^{min} [−]	s^{max} [−]
TES/CTES	0.95	0.95	0.005	4	0	1
BAT	0.96	0.96	0.001	3	0.2	0.8

Appendix A.2. Economic parameters

Tables A.8 and A.9 list all economic parameters of generation and storage technologies. For calculating capital recovery factors, an observation time of 20 years and an interest rate of 5 % is assumed. Additional investments for device replacements as well as residual values at the end of the observation time are considered.

Appendix A.3. Energy purchase costs and feed-in revenues

Gas prices are listed in Table A.11. For electricity, the energy supply price $p_{\mathrm{gas}}^{\mathrm{work}}$ results from a variable EPEX SPOT electricity price (cf. Fig. A.13) as well as several constant portions, such as taxes. The minimum, maximum and average working prices are listed in Table A.12.

The specific feed-in revenue depend on the EPEX SPOT electricity price, monthly average EPEX SPOT prices and the technology (according to German Renewable Energy Sources Act). Characteristic values are shown in Table A.12.

Table A.6: Temperature differences for direct cooling and cooling towers.

$\Delta T_{\mathrm{CT}}^{\mathrm{min}}$ [K]	$\Delta T_{\mathrm{DRC}}^{\mathrm{min}}$ [K]
10	2

Table A.7: Thermal energy storage parameters.

	V_{max} [m^3]	T_{max} [°C]	T_{min} [°C]	$S^{\mathrm{cap,max}}$ [MWh]
TES (BES)	10	90	62	0.325
TES (EH)	100	90	20	8.128
CTES (EH)	100	12	2	1.161

Appendix A.4. Network costs and thermal losses

The network topology is defined by a minimum spanning tree of the graph that directly connects each two buildings. The energy hub is placed at node of building 4 (cf. Fig. 5). Mass flows through the pipes are calculated by solving the system's mass balances. Finally, the pipe diameters and hydraulic pumps are designed based on a maximum pressure gradient of 200 Pa/m. Table A.13 lists the outer and inner pipe diameters D_{a} and D_{i} as well as the corresponding line lengths L and the heat transmittance values kA. The pipe investment I_{Pipes} is approximated based on price lists from different PE-pipe manufacturers. For groundworks, costs of 250 EUR/m are assumed, yielding

$$I_{\mathrm{Pipes}} = \left(250\ \mathrm{EUR/m} + 2293.42\ \mathrm{EUR/m^3} \cdot D_{\mathrm{i}}^2\right) \cdot L \tag{A.1}$$

Economic parameters for pipes are listed in Table A.14.

The kA-values are calculated using $\lambda_{\mathrm{PE}} = 0.4\ \mathrm{W/(m\,K)}$. The thermal resistance of the heat transfer between pipe and soil is calculated according to the European guideline DIN EN 13941 [60].

Table A.8: Economic parameters of generation devices (EH).

	BOI	CHP	EB	CC	AC	CT	PV
Specific investment i $\left[\frac{\text{EUR}}{\text{kW}}\right]$	67.5	750	150	170	525	65	900
Service life t_{L} [a]	20	15	22	15	18	20	20
Capital rec. factor a_{inv} [%]	8.02	9.87	7.75	9.87	8.67	8.02	8.02
Share for o&m f_{om} [%]	3.0	8.0	1.0	3.5	3.0	6.0	1.0

Table A.9: Economic parameters of generation devices (BES).

Parameter	HP	EB	CC	DRC	CT
Specific investment i $\left[\frac{\text{EUR}}{\text{kW}}\right]$	350	150	160	50	65
Service life [a]	20	22	15	30	20
Capital rec. factor a_{inv} [%]	8.02	7.75	9.87	7.02	8.02
Share for o&m f_{om} [%]	2.5	1.0	3.5	3.0	6.0

For hydraulic pumps, specific investments of 500 EUR/kW are used. Further economic parameters are listed in Table A.14. The electric pumping energy is based on the pipe friction factor $f = 0.025$ and the electrical efficiency $\eta_{\text{pumps}} = 0.65$. The total rated electric power of the pumps is 22.82 kW, leading to an annual investment of 1.82 kEUR/a. Their annual electricity demand sums up to 22.4 MWh.

The soil temperature is calculated based on a model by Badache et al. [43]. Considering weather data from the research campus, the course of the year is given by

$$T_{\text{soil}}(t) = 15.32\ ^{\circ}\text{C} - 7.76\ ^{\circ}\text{C} \cos\left(7.17 \cdot 10^{-4} t/\text{h} - 1.144\right) \tag{A.2}$$

The annual heating losses add up to 93.2 MWh, the annual cooling losses to

Table A.10: Economic parameters of energy storages (BES and EH).

	TES/CTES	BAT
Service life t_{L} [a]	20	10
Capital rec. factor a_{inv} [%]	8.02	12.95
Share for o&m f_{om} [%]	2.0	1.0

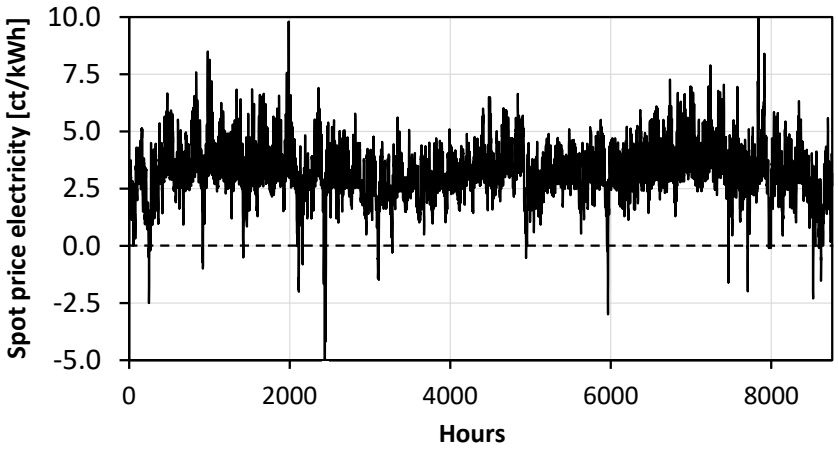

Figure A.13: Hourly price for electricity at EPEX SPOT (2015).

45.7 MWh.

Appendix A.5. Environmental parameters

Table A.15 lists environmental model parameters.

Appendix B. Constraints for direct coolers and cooling towers

In Fig. B.14, the configuration of cooling technologies in the BESs is depicted including the inlet and outlet temperatures. The cooling tower dissipates heat to the environment. The temperature difference between the ambient air temperature and the inlet temperature of the cooling tower

Table A.11: Energy purchase costs.

$p_{\text{gas}}^{\text{cap}}$ [kEUR/MW]	$p_{\text{gas}}^{\text{work}}$ [EUR/MWh]	$p_{\text{el}}^{\text{cap}}$ [kEUR/MW]
12.15	28.24	59.66

Table A.12: Electricity supply costs and feed-in revenues [EUR/MWh].

	$p_{\text{el}}^{\text{work}}$	$r_{\text{feed-in,CHP}}$	$r_{\text{feed-in,CHP}}$
Minimum	28.14	-49.66	-21.34
Maximum	207.85	127.38	152.46
Average	139.79	60.08	85.03

must not be smaller than a certain temperature difference needed for the heat transfer:

$$T_{\text{air}} + \Delta T_{\text{CT}}^{\text{min}} \overset{!}{\leq} T_{\text{CT,in}} = T_{\text{c,ret}} \tag{B.1}$$

Here, the inlet temperature of the cooling tower is equal to the return temperature of the cooling circuit in the building. If Eq. (B.1) is satisfied, the outlet temperature of the cooling tower is

$$T_{\text{CT,out}} = T_{\text{air}} + \Delta T_{\text{CT}}^{\text{min}} \tag{B.2}$$

In order to modulate the cooling power, the cooling tower can be bypassed. This results in a mixing temperature T^* at the outlet of the cooling tower. The cooling power is therefore

$$\dot{Q}_{\text{c,CT}} = \dot{m}_{\text{cool}} c_{\text{p}} \left(T_{\text{c,ret}} - T^* \right) \tag{B.3}$$

$$= \frac{T_{\text{c,ret}} - T^*}{T_{\text{c,ret}} - T_{\text{c,sup}}} \dot{Q}_{\text{c,dem}} \tag{B.4}$$

Here, c_{p} denotes the heat capacity, $\dot{m}_{\text{cool}}$ the mass flow of the building's cooling circuit, and $T_{\text{c,sup}}/T_{\text{c,ret}}$ the supply and return temperature of the

Table A.13: Pipe geometries and costs.

D_a [mm]	D_i [mm]	L [m]	kA $\left[\frac{\mathrm{kW}}{\mathrm{K}}\right]$	I_Pipes [kEUR]	C_Pipes $\left[\frac{\mathrm{kEUR}}{\mathrm{a}}\right]$
75	66.0	150.6	0.38	39.16	2.94
90	79.2	60.66	0.16	16.04	1.21
110	96.8	285.39	0.79	77.48	5.83
125	110.2	188.93	0.54	52.49	3.95
140	123.4	62.03	0.18	17.67	1.33
160	141.0	83.87	0.25	24.79	1.86
180	158.6	93.28	0.29	28.71	2.16
200	176.2	209.45	0.67	67.28	5.06
225	198.2	96.96	0.32	32.98	2.48
250	220.4	114.7	0.39	41.45	3.12
	SUM	1345.9	3.97	398.05	29.93

cooling circuit, respectively.

If the entire mass flow runs through the cooling tower, its maximum cooling power is achieved. In this case, the mixing temperature T^* equals the outlet temperature of the cooling tower:

$$\dot{Q}_{\mathrm{c,CT,max}} = \frac{T_{\mathrm{c,ret}} - T_{\mathrm{CT,out}}}{T_{\mathrm{c,ret}} - T_{\mathrm{c,sup}}} \dot{Q}_{\mathrm{c,dem}} \tag{B.5}$$

From Eq. (B.5), constraint (31) of the LP model can be derived. If the temperature condition (B.1) does not hold, the cooling tower cannot operate, leading to constraint (32).

The direct cooler (DRC) transfers heat into the BLTN. The DRC is modeled in the same way as the cooling tower. Thus, for its operation a temperature condition at the inlet must be satisfied; the inlet temperature $T_{\mathrm{DRC,in}}$

Table A.14: Economic parameters of pipes and hydraulic pumps.

	Pipes	Pumps
Service life t_L [a]	30	10
Capital rec. factor a_inv [%]	7.02	12.95
Share for o&m f_om [%]	0.5	3.0

Table A.15: Environmental parameters.

	Natural gas	Electricity grid
Specific CO_2 emissions e $\left[\frac{\mathrm{kg}}{\mathrm{MWh}}\right]$	201	516
Primary energy factor PEF $\left[\frac{\mathrm{MWh_{PE}}}{\mathrm{MWh}}\right]$	1.1	1.8

is equal to the mixing temperature T^*:

$$T_\mathrm{h}^\mathrm{netw} + \Delta T_\mathrm{DRC}^\mathrm{min} \overset{!}{\leq} T_\mathrm{DRC,in} = T^* \tag{B.6}$$

Since the mixing temperature T^* depends on the cooling power of the cooling tower (which is a decision variable) condition (B.6) can not be evaluated a priori. Instead, the constraint

$$T_\mathrm{h}^\mathrm{netw} + \Delta T_\mathrm{DRC}^\mathrm{min} \overset{!}{\leq} T_\mathrm{c,ret} \tag{B.7}$$

is used to determine time steps of DRC operation. However, the original temperature condition (B.6) still has to be satisfied to enable DRC operation. That is why it is introduced as an additional model constraint as described later on. The DRC outlet temperature is given by

$$T_\mathrm{DRC,out} = T_\mathrm{c}^\mathrm{netw} + \Delta T_\mathrm{DRC}^\mathrm{min} \tag{B.8}$$

Similar to Eq. (B.5), the maximum DRC cooling power is

$$\dot{Q}_\mathrm{c,DRC,max} = \frac{T^* - T_\mathrm{DRC,out}}{T_\mathrm{c,ret} - T_\mathrm{c,sup}} \dot{Q}_\mathrm{c,dem} \tag{B.9}$$

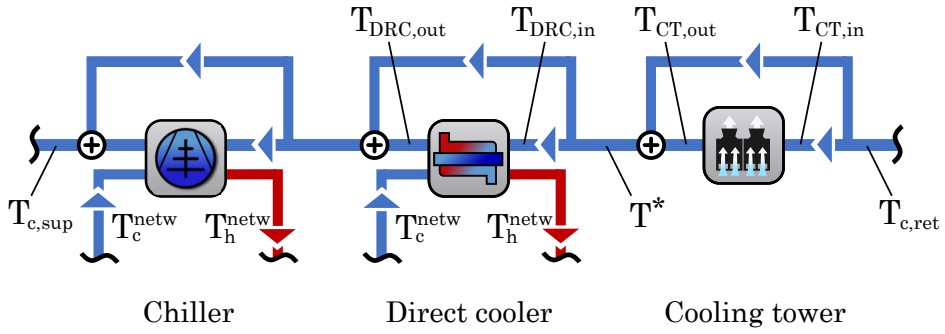

Figure B.14: Cooling generation in building circuit.

The mixing temperature T^* can be obtained by rearranging Eq. (B.4).

$$T^* = T_{\mathrm{c,ret}} - \frac{\dot{Q}_{\mathrm{c,CT}}}{\dot{Q}_{\mathrm{c,dem}}} \left(T_{\mathrm{c,ret}} - T_{\mathrm{c,sup}}\right) \tag{B.10}$$

Hereby, it can be replaced in Eq. (B.9), yielding

$$\dot{Q}_{\mathrm{c,DRC,max}} = \frac{T_{\mathrm{c,ret}} - T_{\mathrm{DRC,out}}}{T_{\mathrm{c,ret}} - T_{\mathrm{c,sup}}} \dot{Q}_{\mathrm{c,dem}} - \dot{Q}_{\mathrm{c,CT}} \tag{B.11}$$

which is used as constraint (34) in the LP. Similarly, T^* can be replaced in the original temperature condition (B.6), leading to

$$T_{\mathrm{h}}^{\mathrm{netw}} + \Delta T_{\mathrm{DRC}}^{\mathrm{min}} \leq T_{\mathrm{c,ret}} - \frac{\dot{Q}_{\mathrm{c,CT}}}{\dot{Q}_{\mathrm{c,dem}}} \left(T_{\mathrm{c,ret}} - T_{\mathrm{c,sup}}\right) \tag{B.12}$$

$$\Leftrightarrow \dot{Q}_{\mathrm{c,CT}} \leq \frac{T_{\mathrm{c,ret}} - \left(T_{\mathrm{h}}^{\mathrm{netw}} + \Delta T_{\mathrm{DRC}}^{\mathrm{min}}\right)}{T_{\mathrm{c,ret}} - T_{\mathrm{c,sup}}} \dot{Q}_{\mathrm{c,dem}} \tag{B.13}$$

which is used as constraint (36) in the LP.

References

[1] European Commission, An EU Strategy on Heating and Cooling (2016). URL https://ec.europa.eu/energy/sites/ener/files/documents/1_EN_ACT_part1_v14.pdf

[2] G. Stryi-Hipp, P. Papillon, K. Mutka, A. Land, B. Sanner, R. Kalf, W. Weiss, 2020-2030-2050, Common vision for the renewable heating and cooling sector in Europe: European technology platform on renewable heating and cooling, Publications Office, Luxembourg, 2011 (2011). doi:10.2788/20474.

[3] H. Lund, B. Möller, B. V. Mathiesen, A. Dyrelund, The role of district heating in future renewable energy systems, Energy 35 (3) (2010) 1381–1390 (2010). doi:10.1016/j.energy.2009.11.023.

[4] H. Lund, S. Werner, R. Wiltshire, S. Svendsen, J. E. Thorsen, F. Hvelplund, B. V. Mathiesen, 4th Generation District Heating (4GDH) Integrating smart thermal grids into future sustainable energy systems, Energy 68 (2014) 1–11 (2014). doi:10.1016/j.energy.2014.02.089.

[5] H. Lund, N. Duic, P. A. Østergaard, B. V. Mathiesen, Future district heating systems and technologies: On the role of smart energy systems and 4th generation district heating, Energy 165 (2018) 614–619 (2018). doi:10.1016/j.energy.2018.09.115.

[6] H. Lund, P. A. Østergaard, M. Chang, S. Werner, S. Svendsen, P. Sorknæs, J. E. Thorsen, F. Hvelplund, B. O. G. Mortensen, B. V. Mathiesen, C. Bojesen, N. Duic, X. Zhang, B. Möller, The status of 4th generation district heating: Research and results, Energy 164 (2018) 147–159 (2018). doi:10.1016/j.energy.2018.08.206.

[7] S. Buffa, M. Cozzini, M. D'Antoni, M. Baratieri, R. Fedrizzi, 5th generation district heating and cooling systems: A review of existing

cases in Europe, Renew Sust Energ Rev 104 (2019) 504–522 (2019). doi:10.1016/j.rser.2018.12.059.

[8] The European Commission, Fifth generation, low temperature, high exergy district heating and cooling networks (2015).
URL https://cordis.europa.eu/project/rcn/194622/factsheet/en

[9] F. Bünning, M. Wetter, M. Fuchs, D. Müller, Bidirectional low temperature district energy systems with agent-based control: Performance comparison and operation optimization, Appl Energy 209 (2018) 502–515 (2018). doi:10.1016/j.apenergy.2017.10.072.

[10] Ruesch F., Rommel M., Scherer J., Pumping power prediction in low temperature district heating networks. Proceedings of International Conference CISBAT 2015, LESO-PB, EPFL, Lausanne. (2015) 753–758 (2015).

[11] A. Prasanna, V. Dorer, N. Vetterli, Optimisation of a district energy system with a low temperature network, Energy 137 (2017) 632–648 (2017). doi:10.1016/j.energy.2017.03.137.

[12] N. Vetterli, M. Sulzer, Dynamic analysis of the low-temperature district network Suurstoffi through monitoring: Proceedings of International Conference CISBAT 2015, LESO-PB, EPFL, Lausanne (2015) 517–522 (2015).

[13] M. Pellegrini, A. Bianchini, The Innovative Concept of Cold District

Heating Networks: A Literature Review, Energies 11 (1) (2018) 236 (2018). doi:10.3390/en11010236.

[14] Stübler A., Bestenlehner D, Drück H., Energy saving potentials of cold district heating networks: Proceedings of the 17th EWA symposium during IFAT 2014, Munich. (2014).

[15] U. Eicker, Urban energy systems for low-carbon cities, Academic Press an imprint of Elsevier, London, 2019 (2019). doi:10.1016/C2016-0-00821-5.

[16] P. Kräuchi, M. Kolb, T. Gautschi, U.-P. Menti, M. Sulzer, Modellbildung füer thermische Arealvernetzung mit IDA-ICE (2014).

[17] M. Sulzer, Kalte Fernwärme (Anergienetze). Grundlagen/Thesenpapier, Hochschule Luzern (2014).

[18] A. Prasanna, N. Vetterli, Modelling the Suurstoffi district based on monitored data to analyse future scenarios for energy self-sufficiency, 19. Status-Seminar Forschen für den Bau im Kontext von Energie und Umwelt (2016).

[19] J. Vivian, X. Jobard, Hassine, I. B., Hurink, J., Smart Control of a District Heating Network with High Share of Low Temperature Waste Heat, 12th Conference on Sustainable Development of Energy, Water and Environmental Systems - SDEWES. October 2017. Dubrovnik, Croatia. (2017).

[20] D. Fischer, Potential for Balancing Wind And Solar Power Using Heat

Pump Heating And Cooling Systems: International Workshop on Integration of Solar into Power Systems. Berlin. (2014).

[21] S. Boesten, W. Ivens, S. C. Dekker, H. Eijdems, 5th generation district heating and cooling systems as a solution for renewable urban thermal energy supply, Advances in Geosciences 49 (2019) 129–136 (2019). doi:10.5194/adgeo-49-129-2019.

[22] R. Rogers, V. Lakhian, M. Lightstone, J. S. Cotton, Modeling of low temperature thermal networks using historical building data from district energy systems, in: Proceedings of the 13th International Modelica Conference, Regensburg, Germany, March 4–6, 2019, pp. 543–550 (2019). doi:10.3384/ecp19157543.

[23] M. Nabeshima, N. Koh, M. Nakao, M. Mike, Estimation of the energy-saving effect of introducing a heat source water network system with single-loop piping utilizing hot spring heat, Energy Procedia 149 (2018) 519–528 (2018). doi:10.1016/j.egypro.2018.08.216.

[24] M. Nakao, M. Nabeshima, Y. Kobayashi, M. Ishinada, Thermal grid system and its field test in multiple buildings with individual heating and cooling facility, Energy Procedia 149 (2018) 112–121 (2018). doi:10.1016/j.egypro.2018.08.175.

[25] D. Wang, K. Orehounig, J. Carmeliet, A Study of District Heating Systems with Solar Thermal Based Prosumers, Energy Procedia 149 (2018) 132 – 140 (2018). doi:10.1016/j.egypro.2018.08.177.

[26] R. Zarin Pass, M. Wetter, M. A. Piette, A thermodynamic analysis of a novel bidirectional district heating and cooling network, Energy 144 (2018) 20–30 (2018). doi:10.1016/j.energy.2017.11.122.

[27] L. Brange, J. Englund, P. Lauenburg, Prosumers in district heating networks – A Swedish case study, Appl Energy 164 (2016) 492–500 (2016). doi:10.1016/j.apenergy.2015.12.020.

[28] F. Ruesch, R. Evins, District heating and cooling with low temperature networks – sketch of an optimization problem, Proceedings of COLEB Workshop, 39–40, 6.-7. March 2014. ETH Zürich. (2014).

[29] E. D. Mehleri, H. Sarimveis, N. C. Markatos, L. G. Papageorgiou, Optimal design and operation of distributed energy systems: Application to Greek residential sector, Renew Energ 51 (2013) 331–342 (2013). doi:10.1016/j.renene.2012.09.009.

[30] H. Harb, J. Reinhardt, R. Streblow, D. Müller, MIP approach for designing heating systems in residential buildings and neighbourhoods, J Build Perform Simu 9 (3) (2016) 316–330 (2016). doi:10.1080/19401493.2015.1051113.

[31] C. Wouters, E. S. Fraga, A. M. James, E. M. Polykarpou, Mixed-integer optimisation based approach for design and operation of distributed energy systems, in: 2014 Australasian Universities Power Engineering Conference (AUPEC), IEEE, 2014, pp. 1–6 (2014). doi:10.1109/AUPEC.2014.6966501.

[32] Q. Wu, H. Ren, W. Gao, J. Ren, Modeling and optimization of distributed energy supply network with power and hot water interchanges, Appl Therm Eng 94 (2016) 635–643 (2016). doi:10.1016/j.applthermaleng.2015.10.157.

[33] A. Omu, R. Choudhary, A. Boies, Distributed energy resource system optimisation using mixed integer linear programming, Energy Policy 61 (2013) 249–266 (2013). doi:10.1016/j.enpol.2013.05.009.

[34] Y. Yang, S. Zhang, Y. Xiao, Optimal design of distributed energy resource systems coupled with energy distribution networks, Energy 85 (2015) 433–448 (2015). doi:10.1016/j.energy.2015.03.101.

[35] C. Wouters, E. S. Fraga, A. M. James, An energy integrated, multi-microgrid, MILP (mixed-integer linear programming) approach for residential distributed energy system planning – A South Australian case-study, Energy 85 (2015) 30–44 (2015). doi:10.1016/j.energy.2015.03.051.

[36] S. Mashayekh, M. Stadler, G. Cardoso, M. Heleno, A mixed integer linear programming approach for optimal DER portfolio, sizing, and placement in multi-energy microgrids, Appl Energy 187 (2017) 154–168 (2017). doi:10.1016/j.apenergy.2016.11.020.

[37] M. Sameti, F. Haghighat, Optimization approaches in district heating and cooling thermal network, Energ Build 140 (2017) 121–130 (2017). doi:10.1016/j.enbuild.2017.01.062.

[38] M. Bohlayer, G. Zöttl, Low-grade waste heat integration in distributed energy generation systems - An economic optimization approach, Energy 159 (2018) 327–343 (2018). doi:10.1016/j.energy.2018.06.095.

[39] T. Schütz, M. H. Schraven, M. Fuchs, P. Remmen, D. Müller, Comparison of clustering algorithms for the selection of typical demand days for energy system synthesis, Renew Energ 129 (2018) 570–582 (2018). doi:10.1016/j.renene.2018.06.028.

[40] F. Domínguez-Muños, J. Cejudo-López, A. Carrillo-Andrés, M. Gallardo-Salazar, Selection of typical demand days for CHP optimization, Energ Build 43 (2015) 3036–3043 (2015). doi:10.1016/j.enbuild.2011.07.024.

[41] VDI 2067-1. Economic efficiency of building installations - Fundamentals and economic calculation. Technical report., Beuth Verlag GmbH (2012).

[42] J. K. Jensen, T. S. Ommen, L. Reinholdt, W. B. Markussen, B. Elmegaard, Heat pump COP, part 2: Generalized COP estimation of heat pump processes, Proceedings of the13th IIR-Gustav Lorentzen Conference on Natural Refrigerants (2018).

[43] M. Badache, P. Eslami-Nejad, M. Ouzzane, Z. Aidoun, L. Lamarche, A new modeling approach for improved ground temperature profile determination, Renew Energ 85 (2016) 436–444 (2016). doi:10.1016/j.renene.2015.06.020.

[44] IEC 61215. Terrestrial photovoltaic (PV) modules - Design qualification and type approval., IEC System of Conformity Assessment Schemes for Electrotechnical Equipment and Components (2016).

[45] P. Gabrielli, M. Gazzani, E. Martelli, M. Mazzotti, Optimal design of multi-energy systems with seasonal storage, Appl Energy 219 (2018) 408–424 (2018). doi:10.1016/j.apenergy.2017.07.142.

[46] L. Kotzur, P. Markewitz, M. Robinius, D. Stolten, Time series aggregation for energy system design: Modeling seasonal storage, Appl Energy 213 (2018) 123–135 (2018). doi:10.1016/j.apenergy.2018.01.023.

[47] Y. Wang, S. You, H. Zhang, W. Zheng, X. Zheng, Q. Miao, Hydraulic performance optimization of meshed district heating network with multiple heat sources, Energy 126 (2017) 603–621 (2017). doi:10.1016/j.energy.2017.03.044.

[48] B. Morvaj, R. Evins, J. Carmeliet, Optimising urban energy systems: Simultaneous system sizing, operation and district heating network layout, Energy 116 (2016) 619–636 (2016). doi:10.1016/j.energy.2016.09.139.

[49] S. Goderbauer, B. Bahl, P. Voll, M. E. Lübbecke, A. Bardow, A. M. Koster, An adaptive discretization MINLP algorithm for optimal synthesis of decentralized energy supply systems, Comput Chem Eng 95 (2016) 38 – 48 (2016). doi:10.1016/j.compchemeng.2016.09.008.

[50] D. E. Hollermann, D. F. Hoffrogge, F. Mayer, M. Hennen, A. Bardow, Optimal (n−1)-reliable design of distributed energy supply sys-

tems, Comput Chem Eng 121 (2019) 317–326 (2019). doi:10.1016/j.compchemeng.2018.09.029.

[51] K. A. Pruitt, R. J. Braun, A. M. Newman, Evaluating shortfalls in mixed-integer programming approaches for the optimal design and dispatch of distributed generation systems, Appl Energy 102 (2013) 386–398 (2013). doi:10.1016/j.apenergy.2012.07.030.

[52] M. Karmellos, G. Mavrotas, Multi-objective optimization and comparison framework for the design of Distributed Energy Systems, Energ Convers Manage 180 (2019) 473–495 (2019). doi:10.1016/j.enconman.2018.10.083.

[53] D. E. Majewski, M. Wirtz, M. Lampe, A. Bardow, Robust multi-objective optimization for sustainable design of distributed energy supply systems, Comput Chem Eng 102 (2017) 26–39 (2017). doi:10.1016/j.compchemeng.2016.11.038.

[54] B. Mohammadi-Ivatloo, F. Jabari, Operation, Planning, and Analysis of Energy Storage Systems in Smart Energy Hubs, Springer International Publishing, Cham, 2018 (2018). doi:10.1007/978-3-319-75097-2.

[55] A. Bischi, L. Taccari, E. Martelli, E. Amaldi, G. Manzolini, P. Silva, S. Campanari, E. Macchi, A detailed MILP optimization model for combined cooling, heat and power system operation planning, Energy 74 (2014) 12–26 (2014). doi:10.1016/j.energy.2014.02.042.

[56] M. A. Rosen, M. N. Le, I. Dincer, Efficiency analysis of a cogeneration

and district energy system, Appl Therm Eng 25 (1) (2005) 147–159 (2005). doi:10.1016/j.applthermaleng.2004.05.008.

[57] S. Jansen, N. Woudstra, Understanding the exergy of cold: theory and practical examples, Int J Exergy 7 (6) (2010) 693–713 (2010). doi:10.1504/IJEX.2010.035516.

[58] HOMER Energy Pro 3.11 Documentation, PV Cell Temperature.
URL https://www.homerenergy.com/products/pro/docs/3.11/how_homer_calculates_the_pv_cell_temperature.html

[59] LG, Fact sheet for PV module type LG360Q1C-A5.
URL https://www.lg.com/global/business/download/resources/solar/DS_NeONR_60cells.pdf

[60] DIN EN 13941: Auslegung und Installation von werkmäßig gedämmten Verbundmantelrohren für die Fernwärme (2010).